

# Beyond Patches: Global-aware Autoregressive Model for Multimodal Few-Shot Font Generation

Haonan Cai<sup>1,2\*</sup> Yuxuan Luo<sup>1\*</sup> Zhouhui Lian<sup>1†</sup>

<sup>1</sup>Wangxuan Institute of Computer Technology, Peking University

<sup>2</sup>School of Electronics Engineering and Computer Science, Peking University

## Abstract

Manual font design is an intricate process that transforms a stylistic visual concept into a coherent glyph set. This challenge persists in automated Few-shot Font Generation (FFG), where models struggle to preserve both structural integrity and stylistic fidelity from limited references. While autoregressive (AR) models have demonstrated impressive generative capabilities, their application to FFG is constrained by conventional patch-level tokenization, which neglects global dependencies crucial for coherent font synthesis. Moreover, existing FFG methods remain within the image-to-image paradigm, relying solely on visual references and overlooking the role of language in conveying stylistic intent during font design. To address these limitations, we propose GAR-Font, a novel AR framework for multimodal few-shot font generation. GAR-Font introduces a global-aware tokenizer that effectively captures both local structures and global stylistic patterns, a multimodal style encoder offering flexible style control through a lightweight language-style adapter without requiring intensive multimodal pretraining, and a post-refinement pipeline that further enhances structural fidelity and style coherence. Extensive experiments show that GAR-Font outperforms existing FFG methods, excelling in maintaining global style faithfulness and achieving higher-quality results with textual stylistic guidance. Project Page: [https://xtryer-s.github.io/projects\\_pages/GAR\\_Font](https://xtryer-s.github.io/projects_pages/GAR_Font)

## 1. Introduction

High-quality fonts are central to visual communication, yet their manual creation is costly: practitioners must translate their design concepts into a full, consistent glyph set. This challenge is compounded for logographic systems like Chinese and Japanese, which contain tens of thousands of characters and complex stroke geometries.

<sup>1\*</sup>: Equal contribution.

<sup>2†</sup>: Corresponding author: lianzhouhui@pku.edu.cn



Figure 1. GAR-Font results under visual and multimodal few-shot settings. The generated poem reflects the key contributions of our model: global-aware tokenization for style fidelity, multimodal style encoding for text-image control, reduced reference requirements, and an autoregressive design that enables controllable high-quality font synthesis.

Few-shot Font Generation (FFG) seeks to automate this process by generating an entire font library from only a handful of reference examples. However, it presents several technical difficulties. First, it demands precise structural fidelity, where strokes, radicals, and local geometry must be correct for every glyph. Second, it requires capturing a holistic and faithful style representation, generalizing from a handful of examples across diverse characters.

A core obstacle for FFG is the lack of an effective visual global representation. GAN-based methods [29, 47] often exhibit noticeable style discrepancies from the reference fonts, and struggle with stroke-level accuracy. Diffusion models [21, 33, 72] improve structural correctness and local fidelity but do not guarantee a coherent global style. Existing sequence approaches such as VQ-Font [73] and IF-Font [13] rely on local patch or block tokenization, which fragments global cues and leads to noticeable discrepancies from the reference styles. Recent autoregressive (AR) image generation methods [25, 76] further reveal the superi-

ority of globally contextualized 1D tokens over 2D patched tokenization, highlighting a promising direction for modeling global stylistic patterns in font synthesis.

Meanwhile, existing FFG methods remain single-modal, using only visual modality for style control. In contrast, linguistic descriptions convey global conceptual design intents beyond visual appearance, providing complementary representations that help overcome the limitations of vision-only models when style must be inferred from a few examples.

These insights motivate GAR-Font, an expressive and controllable FFG framework that integrates visual and linguistic information. Leveraging the AR modeling capacity, GAR-Font introduces three major technical contributions:

- We propose a **global-aware tokenizer (G-Tok)** that fuses local features with global perception, capturing both fine-grained stroke details and font-level style patterns.
- We design an **AR generator with multimodal style encoder**, first pretrained on visual inputs, and then augmented with a lightweight language-style adapter.
- We introduce a **post-refinement pipeline** that improves structural fidelity and stylistic coherence, producing high-quality glyphs from limited references.

To validate the effectiveness of GAR-Font, we conduct extensive experiments across multiple settings. In the standard vision-only scenario, it surpasses other competitive FFG methods, demonstrating superior structural and stylistic fidelity. In the multimodal setting, the augmented multimodal style encoder further improves generation quality. Using 4 reference images plus one textual description, GAR-Font matches the quantitative performance of 8 images while providing flexible control. Ablation studies further confirm that G-Tok produces stable and coherent representations that preserve holistic structure and reference style fidelity—key factors for high-quality font synthesis. GAR-Font moves beyond patch-level modeling by learning global-aware representations and enabling text-driven multimodal FFG, establishing a new AR-based solution for automatic and controllable font generation.

## 2. Related Work

### 2.1. Autoregressive Image Generation

Autoregressive (AR) models have shown powerful generation ability across modalities [1, 32, 38, 42], and their extension to visual generation [14, 49, 53, 54, 61, 62, 75] has demonstrated promising potential. Typically, they follow a two-stage paradigm: a tokenizer encodes images into discrete representations (e.g., VQ-VAEs [50, 59], RQ-VAE [31], VQ-GAN [17, 74]), and a transformer decoder [10, 25, 44, 58, 77] that sequentially predicts these tokens for image reconstruction.

Most AR models use 2D patch-wise tokenization, capturing local details but lacking holistic awareness [5, 12,

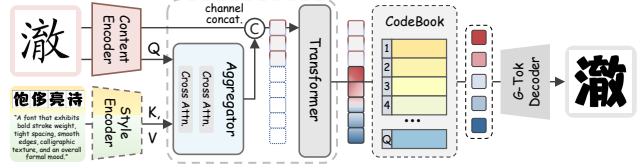


Figure 2. The overall architecture of GAR-Font. It comprises a global-aware tokenizer (G-Tok), and an AR generator, equipped with a multimodal style encoder.

[24, 65]. To improve global coherence, recent works explore complementary strategies: global-context modeling [81] introduces holistic queries for structural reasoning; frequency-domain methods [25, 26] encode coarse-to-fine spectral context; 1D tokenizers [2, 66, 76] enhance efficiency but lose adaptability; semantic tokenization [35, 78] leverages language priors for meaningful visual codes. Structured visual like glyphs, however, demands tokenizers that unify local stroke detail with global aesthetics. Our GAR-Font addresses this challenge through a **global-aware tokenizer** that integrates CNN-based locality with Transformer-based global reasoning, effectively unifying fine-grained stroke detail and overall stylistic coherence.

### 2.2. Few-shot Font Generation

Few-shot Font Generation (FFG) can be broadly divided into vector-based and image-based approaches. Vector FFG methods have progressed in sequential modeling and efficient representations [41, 56, 57, 63, 64, 69]. Yet complex ideographic generation and unseen glyph generalization remain challenging [36, 37]. Image-based methods, in contrast, learn 2D pixel priors for robust adaptation, evolving from early image-to-image translation [4, 9, 11, 67] to more recent VQ and diffusion formulations [33, 34, 72, 73]. These models typically employ content–style disentanglement to separately capture structure and style [8, 19, 21, 22, 39, 46, 48, 71, 79, 80], enhanced by mechanisms like contrastive learning for global coherence [27] and cross-attention for local transfer [55].

The challenge is most acute for glyph-rich, ideographic languages such as Chinese and Korean, where thousands of characters demand fine structure and faithful global style [18, 27, 28, 33]. In this regime, **image-based AR models that operate FFG on globally contextualized visual tokens** show particular promise: by modeling spatial dependencies directly in the 2D domain, they better capture the intricate geometry and visual regularities of glyphs.

### 2.3. Multimodal Alignment for Style Control

Multimodal alignment for style control unifies visual and textual modalities for coherent, fine-grained style manipulation. Foundational models [6, 14, 15, 20, 62, 68] achieve this through costly multimodal pretraining. For fonts, how-

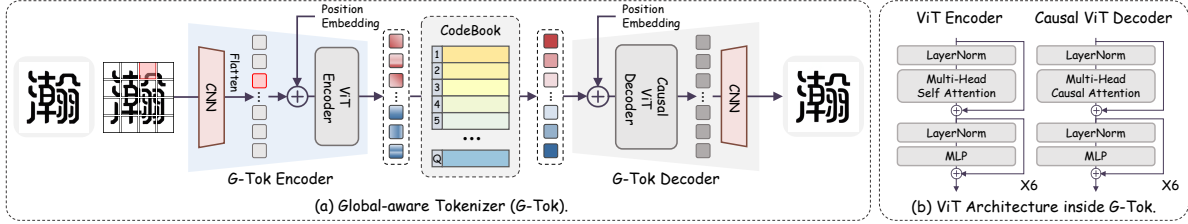


Figure 3. (a) Overview of the G-Tok architecture, which adopts a hybrid CNN–ViT design. (b) Details of the global ViT encoder and causal ViT decoder. With self- and causal-attention, G-Tok captures global dependencies, enabling coherent and high-quality font synthesis.

ever, only textual inputs describing style are incorporated, and the independent encoding of content and style in FFG frameworks [47, 55, 73] naturally forms a structured visual style space that serves as a strong prior for multimodal integration. Recent works pursue efficient alignment via parameter-efficient modules [7, 23, 30, 52] or resampler-based strategies aligning vision and language spaces [1, 40, 43, 70]. Motivated by these works, GAR-Font extends the style encoder in FFG models to a **multimodal style encoder** that consists of a visual style encoder and a lightweight pluggable **language-style adapter** that aligns textual descriptions with visual style embeddings, enabling fine-grained, flexible style control without the need for large-scale multimodal pretraining.

### 3. Method

The architecture of GAR-Font is illustrated in Figure 2. Our framework comprises three core components:

**A global-aware tokenizer (G-Tok)** discretizes glyphs into tokens, capturing intricate structure and global visual style.

**An AR generator with multimodal style encoder** first learns from visual inputs to establish a stable style space, and then employs a lightweight language-style adapter for multimodal style control.

**A post-refinement** enhances structural fidelity and style coherence for high-quality few-shot font generation.

Given a content glyph, a few style references, and optional text, GAR-Font encodes and aggregates content and style, autoregressively generates codebook representations and decodes them softly into high-quality glyphs, which are subsequently improved by a post-refining stage. The details of each module adopted in the proposed GAR-Font will be presented in the following subsections.

#### 3.1. Global-aware Tokenizer

The Global-aware Tokenizer (G-Tok), shown in Figure 3, encodes glyphs into tokens using a hybrid CNN–ViT encoder, a vector quantizer, and a causal hybrid decoder. By fusing local convolutional features with Transformer-based global context, it captures fine-grained structure and overall style, enabling coherent, high-quality font synthesis.

**Hybrid encoding.** Given a glyph image  $\mathbf{I} \in \mathbb{R}^{H \times W \times 3}$ , a CNN encoder  $E_{\text{CNN}}$  extracts local stroke features, which are flattened and aggregated through a ViT encoder  $E_{\text{ViT}}$ :

$$\mathbf{T} = E_{\text{ViT}}(\text{Proj}(E_{\text{CNN}}(\mathbf{I})) + \mathbf{P}_{2\text{D}}) \in \mathbb{R}^{N \times d}, \quad (1)$$

where  $\mathbf{P}_{2\text{D}}$  refers to the 2D sinusoidal position embeddings [16],  $N$  and  $d$  denote token count and embedding dimension. The CNN backbone preserves spatial locality, capturing fine stroke geometry, while the ViT aggregates tokens globally for style fidelity. This hybrid design captures both structure fidelity and long-range style dependencies.

**Vector Quantization.** Following standard VQ-VAE [59] and VQ-GAN [17], we discretize latent tokens by mapping them to the nearest entries in a learnable table. We apply the commitment and embedding regularization with an entropy term to stabilize training and preserve diversity.

**Causal decoding and optimization.** A causal ViT–CNN decoder reconstructs glyph  $\hat{\mathbf{I}}$  from quantized tokens, modeling sequential dependencies while convolutional layers refine local details. Figure 3(b) illustrates this structure.

The tokenizer is optimized end-to-end with weighted reconstruction, perceptual, and vector quantization losses:

$$\mathcal{L}_{\text{tok}} = \lambda_{\text{rec}} \mathcal{L}_{\text{rec}} + \lambda_{\text{per}} \mathcal{L}_{\text{per}} + \lambda_{\text{vq}} \mathcal{L}_{\text{vq}}, \quad (2)$$

where  $\mathcal{L}_{\text{rec}} = \|\mathbf{I} - \hat{\mathbf{I}}\|_1$  denotes the L1 reconstruction loss,  $\mathcal{L}_{\text{per}} = \|\Phi(\mathbf{I}) - \Phi(\hat{\mathbf{I}})\|_2^2$  represents the perceptual loss, and  $\mathcal{L}_{\text{vq}}$  is the standard vector quantization loss.

#### 3.2. AR Generator with Multimodal Style Encoder

Using G-Tok’s global representations, the AR generator performs conditional sequential prediction. To leverage prior FFG insights (Content-style Aggregator) while avoiding the cost of joint image–text training, GAR-Font adopts a decoupled learning paradigm. The generator, aggregator, and style encoder are first trained on visual inputs to learn a stable representation. Based on this foundation, the visual style encoder is extended into a multimodal one through a lightweight, plug-in language adapter that aligns textual cues with learned visual styles, enabling flexible text-guided generation without disturbing the visual prior.

### 3.2.1. Pretraining on Visual Modality

Visualized in Figure 4(a), to build a stable style–content representation, the AR generator is first trained on visual conditions, following the successful practices of prior FFG methods. This ensures robust modeling of both content structure and stylistic variations across glyphs, providing a solid foundation for subsequent multimodal adaptation.

**Encoders and Content–style Aggregator.** As shown in Figure 4(a), we adopt both CNN architectures on the content encoder and the visual style encoder. The Content-style Aggregator follows the previous design [47, 55]. Given a content glyph and  $N_s$  style references, the encoders respectively extract content features  $\mathbf{F}_c$  and style features  $\{\mathbf{F}_{vis_j}\}_{j=1}^{N_s}$ . These features are then fused where content queries attend to fine-grained style cues:

$$\tilde{\mathbf{T}}_{\text{vis}} = \text{Aggregator}(\mathbf{F}_c, \{\mathbf{F}_{vis_j}\}_{j=1}^{N_s}). \quad (3)$$

The aggregated visual representation  $\tilde{\mathbf{T}}_{\text{vis}}$  is concatenated with  $\mathbf{F}_c$  to form the conditioning input  $\mathbf{T}$ .

**Autoregressive modeling and soft decoding.** Conditioned on  $\mathbf{T}$ , the Transformer generator autoregressively predicts the next token, producing logits  $\mathbf{L}$  over the G-Tok codebook  $\mathcal{C}$ . Instead of discrete hard decoding, we apply a soft projection that maps  $\mathbf{L}$  onto the codebook  $\tilde{\mathbf{Z}} = \text{Softmax}(\mathbf{L}) \cdot \mathcal{C}$ . This continuous mapping not only preserves gradient flow during training, enabling pixel-level supervision, but can also improve stroke continuity and glyph fidelity by leveraging the full expressive capacity of the codebook, yielding smoother and more accurate glyphs compared with discrete hard decoding.

**Training objectives.** During this visual-pretraining stage, the aggregator, generator, and style encoder are jointly optimized with a combined token and pixel-level loss:

$$\mathcal{L}_{\text{AR}} = \lambda_{\text{CE}} \mathcal{L}_{\text{CE}} + \lambda_{\text{pixel}} \mathcal{L}_{\text{pixel}}, \quad (4)$$

where  $\mathcal{L}_{\text{CE}}$  is the cross-entropy loss over the target token indices  $s$ , and  $\mathcal{L}_{\text{pixel}}$  measures the L1 reconstruction error between the generated glyph  $\hat{\mathbf{I}}_f$  and ground truth  $\mathbf{I}_f$ .

### 3.2.2. Multimodal Style Encoder Adaptation

Visual pretraining forms a stable style–content space but lacks high-level conceptual control. To address this, we introduce a lightweight, plug-in language adapter that aligns textual design cues with visual style representations, as shown in Figure 4(b). Through this adapter, the style encoder is extended into a multimodal form, enabling flexible text-guided modulation without disrupting the visual prior.

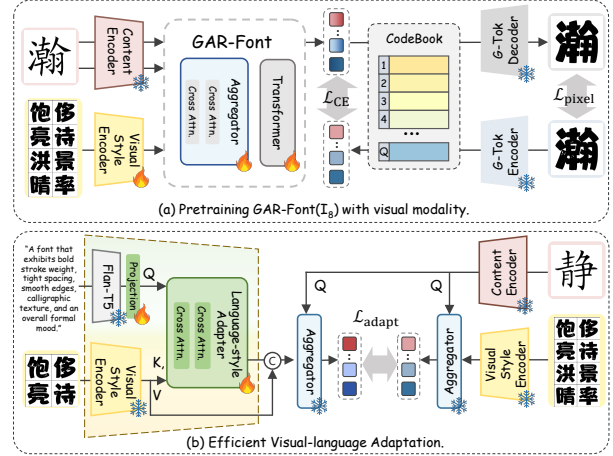


Figure 4. GAR-Font adopts a two-stage training: (a) Visual Pretraining builds a stable content–style space via token and pixel losses; (b) Vision–language Adaptation aligns text embeddings with style features with a lightweight adapter for text-guided generation while preserving visual priors.

**Vision-language Adapter.** The adapter bridges textual descriptions and visual style features through iterative cross-attention. Specifically, a subset of visual style features  $\{\mathbf{F}_{vis_j}\}_{j=1}^k$  is first extracted from  $k < N_s$  reference glyphs by the visual style encoder, while a textual font description embedding is derived from a pretrained Flan-T5 encoder. The text embedding is projected into the visual feature space and iteratively refined by attending to style features. The aligned textual–visual token is then spatially expanded into  $\mathbf{F}_t$  and concatenated with the visual features:

$$\tilde{\mathbf{F}}_{mm} = [\mathbf{F}_{vis_1}, \dots, \mathbf{F}_{vis_k}, \mathbf{F}_t]. \quad (5)$$

**Training objectives.** The multimodal style encoder may produce features  $\tilde{\mathbf{F}}_{mm}$  of different token lengths than the visual-only encoder due to varying numbers of visual references. Thus, we supervise training on their aggregated objectives. Specifically,  $\tilde{\mathbf{T}}_{\text{mm}}$  and  $\tilde{\mathbf{T}}_{\text{vis}}$  are obtained by aggregating  $k$  visual plus one textual reference, and all  $N_s$  visual references, respectively. The adapter is trained by minimizing the  $\ell_2$  distance between these representations:

$$\mathcal{L}_{\text{adapt}} = \|\tilde{\mathbf{T}}_{\text{mm}} - \tilde{\mathbf{T}}_{\text{vis}}\|_2^2. \quad (6)$$

This objective encourages the multimodal encoder to internalize stylistic intent consistent with the full-visual setting, facilitating effective text–style substitution and reducing reliance on visual inputs.

### 3.3. Post-refinement

GAR-Font adopts a two-stage post-refinement to improve few-shot style generalization and structural accuracy: novel font adaptation (NFA) and structural enhancement (SE).

### Novel font adaptation (NFA) for few-shot generalization.

The pretrained generator learns general font patterns but exhibits minor inconsistencies on unseen styles. NFA mitigates this by performing a lightweight adaptation using a few reference glyphs, updating the LoRA layers of the Transformer generator with a mixed token-pixel loss:

$$\mathcal{L}_{\text{NFA}} = \lambda_{\text{CE}} \mathcal{L}_{\text{CE}} + \lambda_{\text{pixel}} \mathcal{L}_{\text{pixel}}, \quad (7)$$

where  $\mathcal{L}_{\text{CE}}$  is the token cross-entropy and  $\mathcal{L}_{\text{pixel}} = \|\mathbf{I} - \hat{\mathbf{I}}\|_1$  encourages pixel-level accuracy. This yields stable few-shot adaptation and better preservation of unseen styles.

### Structural enhancement (SE) for precise glyph reconstruction.

While NFA enhances style fidelity, minor structural distortions may remain. To enhance structural clarity and readability, SE further refines glyphs using a group-relative optimization based on GRPO [51]. The generator is treated as a policy  $\pi_\theta$  that outputs token sequences  $\mathbf{s}$ ; each decoded glyph receives a composite reward:

$$r = \lambda_{\text{ocr}} r_{\text{ocr}} + \lambda_{\text{style}} r_{\text{style}}, \quad (8)$$

where  $r_{\text{ocr}}$  is obtained from a pretrained OCR model as

$$r_{\text{ocr}} = \begin{cases} p_{\text{ocr}}, & \text{if } \hat{y} = y, \\ 0, & \text{otherwise.} \end{cases} \quad (9)$$

Here  $p_{\text{ocr}}$  is the recognition confidence, and  $r_{\text{style}}$  measures the style consistency via a pretrained discriminator.

Rewards are normalized within each sampled group to compute advantages  $A^{(k)} = \frac{r^{(k)} - \mu(r)}{\sigma(r)}$ . SE updates only the LoRA layers by maximizing advantage-weighted likelihood with KL regularization to a frozen reference policy:

$$\mathcal{L}_{\text{SE}} = -\mathbb{E}_{\mathbf{s} \sim \pi_\theta} [A(\mathbf{s}) \log \pi_\theta(\mathbf{s})] + \beta \text{KL}(\pi_\theta \| \pi_{\text{ref}}), \quad (10)$$

where  $A(\mathbf{s})$  denotes the group-normalized advantage and  $\pi_{\text{ref}}$  is the frozen reference policy used for stability.

## 4. Experiments

### 4.1. Datasets and Evaluation Metrics

We evaluate GAR-Font and prior FFG methods on two datasets: a small-scale set containing 440 font styles ( $S$ ) and a large-scale set with 3,040 styles ( $L$ ). The small-scale dataset is a strict subset of the large-scale one, allowing fair cross-scale comparison. In each dataset, we randomly select 40 as unseen test fonts, while the remaining 400 (for  $S$ ) or 3,000 (for  $L$ ) are used for training.

Both datasets are constructed based on the official GB2312 character set, including 6,763 Chinese characters. Among them, 6,251 characters are randomly chosen for

training, and the remaining 512 are held out as unseen characters. During evaluation, we consider two settings:

- (1) *Unseen Fonts Seen Characters (UFSC)*, where 512 seen characters are rendered with the 40 unseen fonts; and
- (2) *Unseen Fonts Unseen Characters (UFUC)*, where 512 unseen characters are rendered with the same unseen fonts.

We use RMSE $\downarrow$ , SSIM $\uparrow$ , LPIPS $\downarrow$ , and FID $\downarrow$  to measure pixel- and perception-level similarity between generated and ground-truth glyphs. Following [33, 47], we train a content classifier over 6,763 characters (99.71% accuracy) and a style classifier over 3,040 fonts (92.72% accuracy) to compute content accuracy (Acc(C) $\uparrow$ ) and style accuracy (Acc(S) $\uparrow$ ). All glyphs are resized to  $64 \times 64$  for evaluation.

### 4.2. Implementation Details

The G-Tok tokenizer discretizes each glyph into 64 tokens using a 2,048-entry, dimension-8 codebook, trained for 200k iterations (batch = 16, lr =  $1 \times 10^{-4}$ ). The vision-only AR generator uses the AdamW optimizer ( $\beta_1 = 0.9$ ,  $\beta_2 = 0.95$ ), conditioned on one Kaiti content. GAR-Font( $I_8$ ) is trained with  $N_s = 8$  style glyphs for 600k/1M iterations on the small/large sets (batch = 32, lr =  $1 \times 10^{-4}$ ).

For multimodal style encoder adaptation, the Language-style Adapter is trained for 40k iterations (batch size = 128, lr =  $1 \times 10^{-4}$ ) with the visual-only features ( $N_s = 8$ ) as ground truth. By adjusting multimodal encoder’s visual style reference numbers  $k = 2/4$ , we build multimodal variants: GAR-Font( $M_2$ ) and GAR-Font( $M_4$ ).

In post-refinement, NFA is conducted on 8 target font glyphs (denoted as NFA-8) for 10 epochs (lr =  $2 \times 10^{-5}$ ). SE is based on GRPO, where each group generates 4 samples and each character is trained with 8 glyphs from different fonts (epochs = 10, batch size = 32, learning rate =  $5e-6$ ).

### 4.3. Comparison on Few-shot Font Generation

We conduct an experiment for **vision-only FFG**, where all models generate glyphs from only reference images. GAR-Font( $I_8$ ) is compared with seven open-source methods: GAN/VAE-based LF-Font [47], VQ-Font [73], DG-Font [71], CF-Font [60]; diffusion-based Diff-Font [21] and Font-Diffuser [72]; and the AR-based IF-Font [13]. All methods are trained and evaluated on the  $S$  and  $L$  datasets using their official resolutions and hyperparameters. GAR-Font( $I_8$ ) is evaluated both before and after post-refinement.

Table 1 shows that GAR-Font( $I_8$ ) consistently outperforms existing vision-only FFG approaches. Even at the pretrained stage, it achieves competitive RMSE $\downarrow$  and SSIM $\uparrow$  on both *UFSC/UFUC*, and obtains the best FID $\downarrow$  scores on the large ( $L$ ) and small ( $S$ ) datasets. With NFA-8 and SE, GAR-Font further improves in both style fidelity and structural accuracy, achieving RMSE $\downarrow$  (0.2503/0.2540) and SSIM $\uparrow$  (0.6411/0.6356) on *UFSC/UFUC*, surpassing existing methods by a large margin.

Table 1. Quantitative results on vision-only FFG. ■ / ■ denote the best results on the *Large* / *Small* datasets, respectively. GAR-Font( $I_8$ ) shows competitive metrics at pretraining and achieves top reconstruction and perceptual performance on the Large UFSC split after NFA-8+SE, demonstrating improved structural fidelity and perceptual quality.

Method	Train	Unseen Fonts Seen Characters (UFSC)						Unseen Fonts Unseen Characters (UFUC)					
		RMSE↓	SSIM↑	LPIPS↓	FID↓	Acc(C)↑	Acc(S)↑	RMSE↓	SSIM↑	LPIPS↓	FID↓	Acc(C)↑	Acc(S)↑
LF-Font	S	0.3984	0.3276	0.2641	32.7464	0.4624	0.0148	0.3983	0.3299	0.2620	32.7028	0.4889	0.0160
	L	0.3988	0.3318	0.2450	21.1028	0.8989	0.0024	0.3986	0.3333	0.2451	21.8141	0.9082	0.0028
VQ-Font	S	<span style="color: blue;">0.2727</span>	<span style="color: blue;">0.5642</span>	0.1830	35.2472	0.8763	0.0016	<span style="color: blue;">0.2744</span>	<span style="color: blue;">0.5616</span>	0.1822	36.7914	0.8882	0.0016
	L	0.2734	0.5633	0.1749	19.3103	0.8549	0.0014	0.2741	0.5627	0.1746	19.971	0.8434	0.0015
DG-Font	S	0.3208	0.4991	0.1281	13.8392	0.9706	0.0764	0.3173	0.5074	0.1270	14.8249	0.9706	0.0797
	L	0.3117	0.5193	0.1235	17.1646	0.9172	0.1089	0.3074	0.5289	0.1214	17.2638	0.9174	0.1120
CF-Font	S	0.3110	0.526	0.1301	18.6961	0.8542	0.0725	0.3077	0.5333	0.1282	19.309	0.8687	0.0747
	L	0.2993	0.5418	0.1155	13.354	0.8931	0.1549	0.2967	0.5474	0.1144	14.0878	0.8947	0.1570
IF-Font	S	0.4076	0.3220	0.1713	14.2393	0.9804	0.0246	0.4063	0.3257	0.1724	14.8211	0.9750	0.0211
	L	0.3969	0.3374	0.1480	11.6470	0.9387	0.1148	0.3949	0.3433	0.1476	11.8445	0.9354	0.1153
Diff-Font	S	0.3688	0.3903	0.1851	10.5722	0.4419	0.0515	-	-	-	-	-	-
	L	0.3651	0.3949	0.1791	9.7051	0.4029	0.1208	-	-	-	-	-	-
Font-Diffuser	S	0.3010	0.4994	0.1728	26.2647	<span style="color: red;">0.9994</span>	0.0212	0.2999	0.5023	0.1720	26.9122	<span style="color: red;">0.9999</span>	0.0226
	L	0.2645	0.5813	0.1419	21.4246	<span style="color: red;">0.9979</span>	0.0527	0.2631	0.5849	0.1407	21.9637	<span style="color: red;">0.9980</span>	0.0578
GAR-Font( $I_8$ )	S	0.3080	0.5052	0.1313	7.9484	0.9408	0.0802	0.3142	0.4932	0.1421	8.4841	0.8993	0.0796
	L	0.2772	0.5799	0.1112	7.7155	0.9146	0.1928	0.2784	0.5787	0.1121	8.0349	0.8912	0.1892
GAR-Font( $I_8$ , +NFA-8)	S	0.2979	0.5418	0.1177	<span style="color: red;">6.6909</span>	0.9195	<span style="color: blue;">0.1128</span>	0.3002	0.5354	0.1195	<span style="color: blue;">6.4693</span>	0.9191	<span style="color: blue;">0.1112</span>
	L	0.2600	0.6158	0.0979	<span style="color: red;">6.5634</span>	0.9210	0.3313	0.2603	0.6160	0.0983	<span style="color: red;">6.5842</span>	0.8921	0.3518
GAR-Font( $I_8$ , +NFA-8+SE)	S	0.2909	0.5619	<span style="color: blue;">0.1111</span>	8.4951	0.9817	0.1101	0.2935	0.5553	<span style="color: blue;">0.1129</span>	8.3504	0.9804	0.1025
	L	<span style="color: red;">0.2503</span>	<span style="color: red;">0.6411</span>	<span style="color: red;">0.0885</span>	8.9851	0.9795	<span style="color: red;">0.3518</span>	<span style="color: red;">0.2540</span>	<span style="color: red;">0.6356</span>	<span style="color: red;">0.0903</span>	8.6602	0.9670	<span style="color: red;">0.3735</span>



Figure 5. Qualitative results on vision-only FFG (UFSC, *Large* dataset). □ / □ indicate structural errors and style mismatches. GAR-Font( $I_8$ , +NFA-8+SE) produces the most faithful glyphs with superior structure and style alignment.

Figure 5 presents comparisons under the *UFSC* setting. GAR-Font( $I_8$ , +NFA-8+SE) generates the most precise and coherent glyphs. By contrast, LF-Font, VQ-Font, DG-Font, CF-Font, and Diff-Font often exhibit stroke distortion or structural collapse on complex styles. IF-Font frequently produces incomplete glyphs with overly thick strokes. Font-Diffuser maintains reasonable structure and style but often shows slight style shifts in the results.

#### 4.4. Efficient Vision-Language Adaptation

We further evaluate **multimodal FFG** to assess whether textual style descriptions can improve over vision-only references. Using GAR-Font( $I_8$ ) on the large ( $L$ ) dataset, we vary the number of visual references  $n_{ref} \in \{2, 4, 8\}$  as baselines. We then introduce multimodal variants GAR-

Font( $M_2$ ) and GAR-Font( $M_4$ ), which pair 2 or 4 visual references with one textual style description. For experimental evaluation, due to the lack of such corpora, Qwen2.5-VL [3] generates descriptions as a proxy of human-authored design intent; details are provided in the supplementary material.

As shown in Table 2, both multimodal models outperform their vision-only counterparts with the same number of visual references across all major metrics. GAR-Font( $M_4$ ) even surpasses the 8-reference visual model, achieving lower RMSE↓/LPIPS↓ and higher SSIM↑ on the *UFSC*, along with a better FID↓ (7.4915 vs. 7.7155). Similar gains appear on *UFUC*, confirming that language provides complementary style cues and reduces reliance on numerous visual references. A mild decrease in ACC(S) is observed, likely because textual guidance yields smoother and

Table 2. Quantitative results on multimodal FFG. GAR-Font( $M_2$ ) and GAR-Font( $M_4$ ) integrate textual style guidance with 2 or 4 visual references, outperforming vision-only baselines across all major metrics. Results demonstrate that language complements visual references, enhancing fine-grained style representation while reducing reliance on handcrafted visuals.

Method	Unseen Fonts Seen Characters (UFSC)						Unseen Fonts Unseen Characters (UFUC)					
	RMSE↓	SSIM↑	LPIPS↓	FID↓	Acc(C)↑	Acc(S)↑	RMSE↓	SSIM↑	LPIPS↓	FID↓	Acc(C)↑	Acc(S)↑
$n_{\text{ref}} = 2$	0.2816	0.5695	0.1158	7.3553	0.9184	0.1535	0.2825	0.5694	0.1162	7.5500	0.8930	0.1619
$n_{\text{ref}} = 4$	0.2807	0.5735	0.1138	7.3781	0.9206	0.1741	0.2813	0.5735	0.1146	<b>7.4880</b>	0.8958	0.1818
$n_{\text{ref}} = 8$	0.2772	0.5799	0.1112	7.7155	0.9146	<b>0.1928</b>	0.2784	0.5787	0.1121	8.0349	0.8912	<b>0.1892</b>
GAR-Font( $M_2$ )	0.2811	0.5724	0.1136	<b>7.3145</b>	<b>0.9296</b>	0.1203	0.2817	0.5731	0.1143	7.5306	<b>0.9068</b>	0.1289
GAR-Font( $M_4$ )	<b>0.2764</b>	<b>0.5825</b>	<b>0.1098</b>	7.4915	0.9260	0.1688	<b>0.2776</b>	<b>0.5816</b>	<b>0.1107</b>	7.6607	0.9039	0.1744

Content	诤	柳	唳	桢	钹	耗	欺	清	吟	饶	尽	瑞	倘	醒	茁	遍	订	钩	坞	弭	之	淑	骥	豕	豎
$n_{\text{ref}} = 2$	诤	柳	唳	桢	钹	耗	欺	清	吟	饶	尽	瑞	倘	醒	茁	遍	订	钩	坞	弭	之	淑	骥	豕	豎
$n_{\text{ref}} = 4$	诤	柳	唳	桢	钹	耗	欺	清	吟	饶	尽	瑞	倘	醒	茁	遍	订	钩	坞	弭	之	淑	骥	豕	豎
$n_{\text{ref}} = 8$	诤	柳	唳	桢	钹	耗	欺	清	吟	饶	尽	瑞	倘	醒	茁	遍	订	钩	坞	弭	之	淑	骥	豕	豎
Textual style description	"A font that exhibits sharp strokes and angular rhythm, conveying energy and tension."					"A font that features smooth curves and gentle flow, evoking warmth and elegance."					"A font that combines graceful brush rhythm with open spacing, expressing a calm and refined charm."					"A font that blends dynamic brushwork with balanced structure, showing lively yet stable form."					"A font that presents bold, square strokes and solid geometry, reflecting order and strength."				
GAR-Font( $M_2$ )	诤	柳	唳	桢	钹	耗	欺	清	吟	饶	尽	瑞	倘	醒	茁	遍	订	钩	坞	弭	之	淑	骥	豕	豎
GAR-Font( $M_4$ )	诤	柳	唳	桢	钹	耗	欺	清	吟	饶	尽	瑞	倘	醒	茁	遍	订	钩	坞	弭	之	淑	骥	豕	豎
Target	诤	柳	唳	桢	钹	耗	欺	清	吟	饶	尽	瑞	倘	醒	茁	遍	订	钩	坞	弭	之	淑	骥	豕	豎

Figure 6. Qualitative results on multimodal FFG(UFSC, *Large* dataset).   denotes local slight structural mistakes and   marks samples with stylistic regression. With textual style guidance, GAR-Font( $M_2$ ) and GAR-Font( $M_4$ ) yield more structurally accurate and stylistically coherent generations, demonstrating enhanced stable fine-grained style control compared to vision-only baselines (*first three rows*).

more diverse styles beyond the classifier’s limit.

Qualitative examples in Figure 6 show that GAR-Font( $M_2$ ) and GAR-Font( $M_4$ ) preserve styles more reliably than vision-only models, particularly when  $n_{\text{ref}} = 2$ , where the visual baseline noticeably drifts toward generic shapes. This highlights the effectiveness of language in reinforcing style fidelity under low-reference conditions.

## 4.5. Ablation Studies

### 4.5.1. On G-Tok’s Hybrid Architecture

To validate G-Tok’s hybrid CNN-ViT design, we start from a CNN-based tokenizer [53] and progressively insert ViT blocks at different depths to introduce global awareness.

We conduct two complementary analyses on *UFUC* test:

- Linear Probing** evaluates the discriminative quality of frozen G-Tok representations for style and content prediction using a single-layer linear classifier. Features are extracted and flattened from the frozen tokenizer encoder, and high classification accuracy indicates that the encoder effectively captures and discriminates structural and stylistic information.
- Reconstruction Robustness** recovers glyphs corrupted by localized Gaussian noise ( $\sigma = 0.2$ , affecting 20% of the glyph area). High performance indicates that the tokenizer effectively preserves global structure and stylistic cues despite local perturbations.

Table 3 shows that the pure ViT excels in linear probing

Table 3. Ablation of G-Tok’s hybrid CNN-ViT architecture on *UFUC*(*Small* dataset). **Bold** and underline indicate the best and second-best results. Progressive integration of attention improves both discriminative representation and reconstruction fidelity.

Method	Linear Probing		Reconstruction Robustness			
	Acc(S)↑	Acc(C)↑	RMSE↓	SSIM↑	LPIPS↓	FID↓
CNN	0.5515	0.3879	0.1167	0.8535	0.0423	28.4279
ViT-6	<b>0.6907</b>	<b>0.5334</b>	0.1636	0.7333	0.0933	98.4270
CNN-ViT-2	0.5229	0.3772	0.1114	0.8552	<u>0.0420</u>	30.0034
CNN-ViT-4	0.5585	0.3667	<u>0.1114</u>	<u>0.8563</u>	0.0430	<u>24.7323</u>
CNN-ViT-6	<u>0.6277</u>	<u>0.4897</u>	<b>0.1088</b>	<b>0.8594</b>	<b>0.0412</b>	<b>22.1577</b>

Table 4. Ablation of G-Tok’s architecture on *UFUC*(*Small* dataset). Incorporating self-attention (CNN+Non-Causal ViT) improves global modeling while causal attention further strengthens sequential modeling, yielding the best overall performance.

Method	RMSE↓	SSIM↑	LPIPS↓	FID↓	Acc(C)↑	Acc(S)↑
CNN	0.3447	0.4350	0.1728	10.5239	0.6722	0.0221
CNN+Non-Causal ViT	0.3271	0.4745	0.1562	8.7504	0.8019	0.0436
CNN+Causal ViT	<b>0.3142</b>	<b>0.4932</b>	<b>0.1421</b>	<b>8.4841</b>	<b>0.8993</b>	<b>0.0796</b>

but suffers in reconstruction, while the CNN baseline ensures stable recreation with weaker probing results. The hybrid G-Tok progressively integrates global attention, with the CNN-ViT-6 variant achieving the best, improving both classification accuracy and reconstruction fidelity across all metrics. Visualizations are in the supplementary material.

Table 5. Ablation of decoding strategy and pixel-level supervision on UFSC and UFUC(*Small* dataset). Soft decoding outperforms hard decoding across all metrics, and pixel supervision further enhances reconstruction fidelity and recognition accuracy.

Training Loss	Decoding Strategy	Unseen Fonts Seen Characters (UFSC)						Unseen Fonts Unseen Characters (UFUC)					
		RMSE↓	SSIM↑	LPIPS↓	FID↓	Acc(C)↑	Acc(S)↑	RMSE↓	SSIM↑	LPIPS↓	FID↓	Acc(C)↑	Acc(S)↑
w/o pixel loss	hard	0.3235	0.4679	0.1517	10.3181	0.8647	0.0377	0.3322	0.4510	0.1602	11.2142	0.7465	0.0396
	soft	0.3231	0.4745	0.1502	9.6696	0.9171	0.0426	0.3313	0.4583	0.1589	10.3813	0.8104	0.0430
w/ pixel loss	hard	0.3083	0.4991	0.1329	8.3024	0.9032	0.0771	0.3157	0.4862	0.1448	8.9043	0.8404	0.0680
	soft	<b>0.3080</b>	<b>0.5052</b>	<b>0.1313</b>	<b>7.9484</b>	<b>0.9408</b>	<b>0.0802</b>	<b>0.3142</b>	<b>0.4932</b>	<b>0.1421</b>	<b>8.4841</b>	<b>0.8993</b>	<b>0.0796</b>

Table 6. Quantitative comparison of joint training (GAR-Font( $VL_k$ )) versus the decoupled adapter scheme (GAR-Font( $M_k$ )) on unseen fonts. The decoupled Language-style Adapter surpasses joint-trained multimodal encoders, validating more effective vision–language alignment and improved reconstruction and perceptual metrics.

Method	Unseen Fonts Seen Characters (UFSC)						Unseen Fonts Unseen Characters (UFUC)					
	RMSE↓	SSIM↑	LPIPS↓	FID↓	Acc(C)↑	Acc(S)↑	RMSE↓	SSIM↑	LPIPS↓	FID↓	Acc(C)↑	Acc(S)↑
GAR-Font( $VL_2$ )	0.3070	0.5124	0.1458	10.7566	0.8552	0.1104	0.3100	0.5087	0.1473	11.0381	0.7979	0.1209
GAR-Font( $VL_4$ )	0.2983	0.5378	0.1279	7.9272	0.8970	0.1165	0.3006	0.5351	0.1290	8.1126	0.8665	0.1216
GAR-Font( $M_2$ )	0.2811	0.5724	0.1136	<b>7.3145</b>	<b>0.9296</b>	0.1203	0.2817	0.5731	0.1143	<b>7.5306</b>	<b>0.9068</b>	0.1289
GAR-Font( $M_4$ )	<b>0.2764</b>	<b>0.5825</b>	<b>0.1098</b>	7.4915	0.9260	<b>0.1688</b>	<b>0.2776</b>	<b>0.5816</b>	<b>0.1107</b>	7.6607	0.9039	<b>0.1744</b>

#### 4.5.2. On G-Tok’s Global and Causal Modeling

We further ablate G-Tok’s ViT architecture to assess its global and causal modeling. We pretrain three visual AR variants that differ in G-Tok and examine them on *UFUC*:

1. **CNN**: a baseline CNN tokenizer without global context;
2. **CNN + Non-causal ViT**: a hybrid CNN-ViT tokenizer with self-attention that only supports global interaction;
3. **CNN + Causal ViT**: full G-Tok, hybrid CNN-ViT tokenizer with causal self-attention for sequential modeling.

Table S6 shows that incorporating self-attention ViT improves performance over the CNN baseline, while the causal ViT further enhances sequential modeling, achieving the best results across all metrics. Detailed *UFSC* results are provided in the supplementary material.

#### 4.5.3. On AR Generator’s Soft-decoding

To validate the effectiveness of pixel-level supervision and the soft decoding strategy, we conduct ablation experiments on our vision-only generator. The results in Table 5 demonstrate that soft decoding achieves superior performance over all metrics, particularly when combined with pixel-level supervision. This combination yields the lowest RMSE↓, LPIPS↓, and FID↓ while achieving the highest SSIM↑ and classifier accuracies on *UFSC* and *UFUC*, indicating improved pixel-level fidelity and faithful style preservation.

#### 4.5.4. On Multimodal Style Encoder’s Adaptation

GAR-Font adopts a decoupled training paradigm: a visual encoder is pretrained, followed by multimodal control via a lightweight adapter. To validate this design, we compare it with jointly training a multimodal style encoder under the same configuration on the large ( $L$ ) dataset.

We evaluate two joint training variants, **GAR-Font( $VL_2$ )** and **GAR-Font( $VL_4$ )**, against the decoupled multimodal variants **GAR-Font( $M_2$ )** and **GAR-Font( $M_4$ )**.

As Table 6 shows, decoupled variants consistently outperform joint-trained counterparts under the same number of visual references. For example, GAR-Font( $M_4$ ) attains the best RMSE↓, LPIPS↓, and SSIM↑ on *UFSC / UFUC*, while GAR-Font( $VL_4$ ) performs worse. GAR-Font( $M_2$ ) also achieves the best FID↓ on *UFSC* (7.3145). These results validate the decoupled vision–language training paradigm, where a pretrained visual encoder and a lightweight adapter achieve efficient and robust text–visual alignment, improving generalization in multimodal FFG.

#### 4.6. Limitations and Future Work

Although GAR-Font surpasses existing FFG methods in visual fidelity, several limitations remain. First, the Multimodal Style Encoder currently relies on late adaptation via a language-style adapter; exploring earlier text-image fusion may enable finer stylistic control and reduce reliance on visual references. Second, our experiments are conducted at a resolution of  $64 \times 64$ , which may limit direct applicability to high-DPI scenarios; extending the framework to higher resolutions may require G-Tok to handle longer token sequences. Finally, we aim to expand controllability beyond style and content, adding attributes like stroke thickness, character width, and slant for more flexible font generation.

### 5. Conclusion

In this paper, we present GAR-Font, a global-aware autoregressive framework for few-shot font generation that combines a hybrid global tokenizer, an autoregressive generator with a multimodal style encoder, and a post-refinement pipeline. GAR-Font achieves superior structural and stylistic fidelity, outperforming prior vision-only baselines, while demonstrating that language-guided adaptation can rival or exceed heavy visual conditioning with improved flexibility.

## **Acknowledgments**

This work was supported by National Natural Science Foundation of China (Grant No.: 62372015), Leading Projects in Key Research Fields of Language Funded by the National Language Commission, Center For Chinese Font Design and Research, Key Laboratory of Intelligent Press Media Technology, and National Engineering Research Center of New Electronic Publishing Technologies.

# Beyond Patches: Global-aware Autoregressive Model for Multimodal Few-Shot Font Generation

## Supplementary Material

### A. Overview

This supplementary material provides additional details on dataset construction, implementation, and extended experiments supporting the main paper. The sections are organized as follows:

- **Sec. B:** Model configurations of G-Tok, the autoregressive generator, and the multimodal style encoder.
- **Sec. C:** Data curation and partitioning, covering both training and evaluation protocols.
- **Sec. D:** Extended quantitative results, including scaling analyses of our autoregressive generator.
- **Sec. E:** Detailed and visualized ablations of key design choices in GAR-Font.
- **Sec. F:** Qualitative results for visual-only and multimodal FFG, cross-language, and higher-resolution generation.
- **Sec. G:** Analysis of GAR-Font failure cases in dense-stroke and complex font styles.

### B. Model Configuration

Tab. S1 details the architectural specifications of GAR-Font. The framework relies on three core components: (1) The **Global-aware Tokenizer (G-Tok)**, which employs a hybrid CNN-ViT to discretize glyphs into a compact codebook; (2) The **Autoregressive Generator**, which serves as the synthesis backbone, using a Transformer decoder to predict tokens conditioned on aggregated content and style features; and (3) The **Multimodal Style Encoder**, which utilizes a lightweight adapter to align textual embeddings with visual style features for text-driven control.

### C. Data Curation

#### C.1. Data Collection and Statistics

We construct a comprehensive font dataset derived from the official GB2312 character set. As illustrated in Fig. S1, the whole training and test dataset is structured as a matrix spanned by two orthogonal axes: *Font Style* (vertical axis) and *Character Category* (horizontal axis). The collected data comprises 3,040 fonts and 6,763 characters.

For training data, along the Character Axis, we split 6,251 training characters (left column) and 512 characters unseen (right column). The unseen characters are reserved strictly for testing to evaluate the model’s capability to generate novel glyph structures. Similarly, the font library is divided into 3,000 training fonts (top rows) and 40 unseen test fonts (bottom rows).

Key Components	Params (M)
<b>G-Tok</b>	79.59
CNN Encoder	28.56
ViT Encoder (layers = 6)	4.73
Codebook (size = 2048, dim = 8)	0.02
ViT Decoder (layers = 6)	4.73
CNN Decoder	41.42
<b>AR-Generator</b>	346.23
Content Encoder	28.56
Visual Style Encoder	2.78
Content-style Aggregator (layers = 3)	0.79
Transformer Decoder (layers = 24)	314.10
<b>Multimodal Style Encoder</b>	8.04
Projection	0.52
Visual Style Encoder	2.78
Language-Style Adapter (layers = 6)	4.74

Table S1. Key GAR-Font components and parameter counts.

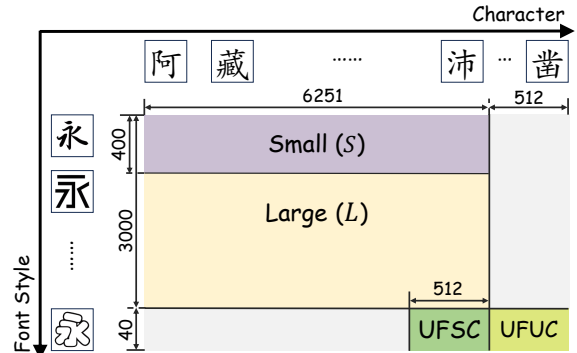


Figure S1. **Visual illustration of the dataset partition.** The data is organized along font and character axes. Pre-training utilizes the purple and yellow regions ( $S$  and  $L$ ). Evaluation is conducted on the bottom green regions ( $UFSC$  and  $UFUC$ ), strictly isolating unseen styles and characters.

#### C.2. Pretraining Data

The pretraining phase utilizes the data located in the upper-left quadrant of Fig. S1, defined by the intersection of training fonts and training characters. Within this quadrant, we define two configurations to investigate scaling behaviors:

- **Large ( $L$ ):** The full training block consisting of all 3,000 training fonts paired with the 6,251 training characters (represented by the blue region).
- **Small ( $S$ ):** A subset consisting of the first 400 training fonts paired with the same 6,251 characters (represented by the reddish overlay).

Training on  $S$  versus  $L$  allows us to assess the model’s data efficiency and performance scaling with respect to the diversity of source styles.

### C.3. Textual Prompt Collection

To support multimodal few-shot font generation (FFG), we construct a consistent textual prompt set that captures font-level stylistic attributes. Since human-authored font design descriptions are not available in existing datasets, we automatically generate textual prompts to approximate human design intent. For each font, we randomly sample 40 glyph images and jointly input them into Qwen2.5-VL. The model is instructed to produce a single, unified description summarizing only the visual properties that remain consistent across the full glyph set—such as stroke weight, curvature, structural proportions, spatial rhythm, edge texture, and overall tonal characteristics. This process yields a controlled and stylistically coherent textual representation for each font.

The exact prompt used for textual description extraction is provided below:

**Textual Style Description Collection Prompt**

You are an experienced typographic style analyst. You are given a set of glyph images belonging to the same font. Your task is to synthesize a unified stylistic description that captures only the consistent, font-level visual attributes shared across the full glyph set.

Your output must adhere to the following specifications:

**1. Required Format**  
Provide a single paragraph that:

- begins with the phrase “A font that ...”,
- contains approximately 45–50 words,
- includes only stylistic properties observable across all glyphs,
- avoids speculative or uncertain expressions.

**2. Allowed Stylistic Dimensions**  
Constrain your analysis to the following attributes:

- stroke weight (light, medium, bold, uniform, contrasting),
- curvature (straight, angular, rounded, flowing, sharp),
- structural proportions (compact, tall, wide, balanced),
- spacing and rhythm (tight, loose, even, irregular),
- edge rendering (smooth, sharp, rough, brush-like),
- overall tone or mood (elegant, modern, classical, playful, gentle, formal).

**3. Constraints**  
All statements must be visually grounded in the provided glyph set. Do not reference features specific to individual characters. The description must reflect global stylistic coherence and maintain typographic precision.

### C.4. Post-Refinement Data

To further adapt the model to novel styles and enhance structural consistency, we employ specific data subsets:

**Novel Font Adaptation (NFA).** NFA adapts the pre-trained model to the style of the 40 unseen test fonts. For each test font, we sample 8 characters (NFA-8) from the 6,251 training character set to serve as style references. This process operates within the vertical column of the training characters but focuses on the unseen font rows.

**Structural Enhancement (SE).** SE aims to consolidate global glyph consistency. It utilizes the entire 6,763 characters (spanning both training and unseen characters) but restricts the style to a manageable subset of 400 fonts (sampled from

Table S2. Quantitative evaluation on VQ-Font vs. VQ-Font (G). Replacing the original VQ-VAE with G-Tok halves the FID score and boosts content accuracy by nearly 9%.

Unseen Fonts Seen Characters (UFSC)						
Method	RMSE↓	SSIM↑	LPIPS↓	FID↓	Acc(C)↑	Acc(S)↑
VQ_Font	0.2727	0.5642	0.1830	35.2472	0.8763	0.0016
VQ_Font (G)	<b>0.2725</b>	<b>0.5644</b>	<b>0.1731</b>	<b>17.3296</b>	<b>0.9646</b>	<b>0.0022</b>
Unseen Fonts Unseen Characters (UFUC)						
Method	RMSE↓	SSIM↑	LPIPS↓	FID↓	Acc(C)↑	Acc(S)↑
VQ_Font	0.2744	0.5616	0.1822	36.7914	0.8882	0.0016
VQ_Font (G)	<b>0.2732</b>	<b>0.5637</b>	<b>0.1731</b>	<b>17.9152</b>	<b>0.9653</b>	<b>0.0023</b>

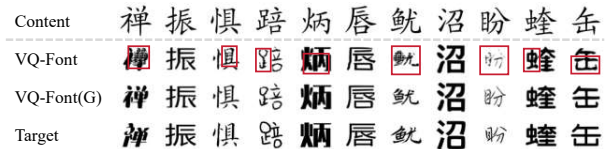


Figure S2. Qualitative comparison on VQ-Font vs. VQ-Font (G).  marks structural errors in the generated glyph. G-Tok improves structure preservation and produces more faithful font styles.

$S$ ). This ensures the model sees a complete range of structural geometries during the refinement phase without the computational cost of the full font library.

### C.5. Evaluation Data

Evaluation is strictly conducted on the held-out bottom rows of the matrix (Fig. S1), ensuring no overlap with the pre-training data. We define two rigorous settings:

- **UFSC** (Unseen Fonts, Seen Characters): Represented by the light green region. This setting evaluates the model’s ability to stylize known characters into novel font styles.
- **UFUC** (Unseen Fonts, Unseen Characters): Represented by the dark green region. This is the most challenging zero-shot setting, where the model must generate glyphs that are novel in both style and structure.

## D. More Quantitative Experiments

### D.1. Adaptation on G-Tok to Other FFG Methods

To verify the versatility of our G-Tok, we integrated it into VQ-Font by replacing its native VQ-VAE with our G-Tok while maintaining the original model architecture and configuration. The modified model, **VQ-Font (G)**, was trained on the Small dataset with G-Tok. As shown in Tab. S2, this simple replacement yields significant improvements across all metrics. Most notably, FID↓ decreases by nearly 50% (e.g., 35.25 → 17.33 on UFSC) and Content Accuracy↑ improves by approximately 9% (~ 87% → ~ 96%). These substantial gains demonstrate that G-Tok’s

Table S3. Quantitative results of NFA glyph number ablation for few-shot font adaptation. Increasing from NFA-8 to NFA-128 consistently improves style faithfulness and perceptual quality. Applying SE further enhances structural fidelity.

Method	Train	Unseen Fonts Seen Characters (UFSC)						Unseen Fonts Unseen Characters (UFUC)					
		Set	RMSE↓	SSIM↑	LPIPS↓	FID↓	Acc(C)↑	Acc(S)↑	RMSE↓	SSIM↑	LPIPS↓	FID↓	Acc(C)↑
NFA-8	S	0.2979	0.5418	0.1177	6.6909	0.9195	0.1128	0.3002	0.5354	0.1195	6.4693	0.9191	0.1112
	L	0.2600	0.6158	0.0979	6.5634	0.9210	0.3313	0.2603	0.6160	0.0983	6.5842	0.8921	0.3518
NFA-8+SE	S	0.2909	0.5619	0.1111	8.4951	0.9817	0.1101	0.2935	0.5553	0.1129	8.3504	0.9804	0.1025
	L	0.2503	0.6411	0.0885	8.9851	0.9795	0.3518	0.2540	0.6356	0.0903	8.6602	0.9670	0.3735
NFA-32	S	0.2880	0.5598	0.1095	5.7662	0.8993	0.1786	0.2849	0.5679	0.1075	5.8886	0.8962	0.1978
	L	0.2561	0.6238	0.0949	6.1329	0.9093	0.3707	0.2570	0.6234	0.0957	6.1493	0.8758	0.3946
NFA-32+SE	S	0.2803	0.5821	0.1028	7.1792	0.9734	0.1754	0.2781	0.5878	0.1012	7.1134	0.9724	0.1970
	L	0.2455	0.6515	0.0854	8.2308	0.9775	0.4048	0.2460	0.6513	0.0862	7.8937	0.9581	0.4342
NFA-128	S	0.2712	0.5933	0.0992	5.4254	0.9236	0.3179	0.2836	0.5702	0.1079	5.6667	0.8817	0.3277
	L	0.2435	0.6507	0.0855	5.7570	0.9228	0.4457	0.2496	0.6397	0.0904	5.8078	0.8830	0.4625
NFA-128+SE	S	0.2671	0.6089	0.0948	6.9103	0.9718	0.2833	0.2788	0.5884	0.1022	7.1309	0.9242	0.2958
	L	0.2398	0.6627	0.0831	8.3751	0.9776	0.4154	0.2508	0.6377	0.0908	7.2034	0.9068	0.4183

Table S4. Quantitative results of GAR-Font (M2/M4) across different description sources and formats under UFSC. M2/M4 denote inference with 2/4 reference glyphs plus text. All results outperform the corresponding non-text baselines in Table 2.

Method	Variants	RMSE↓	SSIM↑	LPIPS↓	FID↓	Acc(C)↑	Acc(S)↑
<b>SmolVLM2-2.2B (Fixed-Template)</b>	M2	0.2768	0.5819	0.1111	7.9185	0.9143	0.1384
	M4	0.2732	0.5878	0.1088	7.4247	0.9206	0.1747
<b>Qwen2.5-VL (Free-Form)</b>	M2	0.2765	0.5808	0.1110	7.7404	0.9263	0.1329
	M4	0.2730	0.5890	0.1095	6.9813	0.9016	0.1702

hybrid CNN-ViT architecture captures far richer structural and stylistic semantics than standard VQ-VAEs, serving as a robust plug-and-play enhancement for quantization-based FFG methods. Fig. S2 illustrates that integrating G-Tok helps the model preserve coherent global structures for complex fonts and generate styles that better align with the target font, indicating a richer and more semantically stable global representation G-Tok than the original VQ-VAE.

## D.2. Effect of the Number of NFA Glyphs

In Section 4.3, we adopt NFA-8 to maintain a strict few-shot adaptation setting. We further investigate the impact of using more adaptation glyphs by extending the setting to NFA-32 and NFA-128.

As visualized in Tab. S3, increasing the number of adaptation glyphs consistently improves the style modeling and perceptual quality. Style Accuracy (Acc(S)↑) rises notably from NFA-8 to NFA-128 on both UFSC and UFUC, indicating that additional glyphs provide richer stylistic cues for capturing font-specific characteristics. Notably, on the *Large* dataset, NFA-128 achieves the highest style accuracy (0.4457 on UFSC and 0.4625 on UFUC), substantially outperforming NFA-8. These results suggest that despite the NFA-8 setting adopted in the main paper already provides a strong and practical few-shot configuration, more NFA

glyphs further refine the font transfer quality.

## D.3. Robustness Across Textual Description Sources

In Section 4.4, multimodal experiments are conducted using the generated descriptions of Qwen2.5-VL with the fixed-form template in Section C.3. To validate the robustness of our approach, we further evaluate GAR-Font using two types of descriptions: a free-form prompt for Qwen2.5-VL and the fixed-template prompt for SmolVLM2-2.2B-Instruct [45], each generated using only 8 reference glyphs.

Tab. S4 shows the multimodal gains are consistent across description sources and formats. GAR-Font( $M_2/M_4$ ) outperforms corresponding non-text baselines, demonstrating that our vision-language adaptation is robust to variations in prompt style and source model.

## D.4. Post-Refinement of Multimodal FFG

In Section 4.4, we demonstrated the efficacy of GAR-Font( $M_2/M_4$ ) on multimodal FFG, but limited to pretraining stage. To fully assess the potential of our lightweight vision-language adaptation, we extend the evaluation to the complete pipeline. We apply our NFA-128 and SE stages to both the vision-only baselines and our multimodal variants. All models are trained on the Large (*L*) dataset.

As visualized in Tab. S5, the inclusion of textual descriptions significantly enhances the effectiveness of the post-refinement stage. Unlike the pre-training phase where multimodal models showed a slight dip in style accuracy (Acc(S)↑), the fully refined GAR-Font( $M_2$ ) and GAR-Font( $M_4$ ) exhibit a substantial lead in Acc(S)↑ compared to their vision-only counterparts ( $n_{\text{ref}} = 2$  and  $n_{\text{ref}} = 4$ ). Notably, **GAR-Font( $M_4$ ) outperforms the 8-reference vision-only baseline ( $n_{\text{ref}} = 8$ )** across most key metrics, including RMSE↓, SSIM↑, LPIPS↓, and Style Accuracy↑ (0.4566 vs. 0.4154 on *UFSC*).

Table S5. Quantitative evaluation of Multimodal FFG with full post-refinement (NFA and SE) on Unseen Fonts. All models listed are post-trained with NFA-128 and SE stages on the Large dataset.

Method	Unseen Fonts Seen Characters (UFSC)						Unseen Fonts Unseen Characters (UFUC)					
	RMSE↓	SSIM↑	LPIPS↓	FID↓	Acc(C)↑	Acc(S)↑	RMSE↓	SSIM↑	LPIPS↓	FID↓	Acc(C)↑	Acc(S)↑
$n_{\text{ref}} = 2$	0.2501	0.6438	0.0888	10.1464	<b>0.9851</b>	0.3314	0.2701	0.5987	0.1069	9.4294	0.8720	0.3433
$n_{\text{ref}} = 4$	0.2437	0.6552	0.0848	9.5960	0.9839	0.3711	0.2692	0.6007	0.1049	9.0877	0.8828	0.3835
$n_{\text{ref}} = 8$	0.2398	0.6627	0.0831	<b>8.3751</b>	0.9776	0.4154	<b>0.2508</b>	<b>0.6377</b>	<b>0.0908</b>	<b>7.2034</b>	<b>0.9068</b>	0.4183
GAR-Font( $M_2$ )	0.2361	0.6707	0.0799	8.8867	0.9817	0.4508	0.2527	0.6352	0.0909	8.1444	0.9029	0.4247
GAR-Font( $M_4$ )	<b>0.2358</b>	<b>0.6712</b>	<b>0.0796</b>	8.8073	0.9800	<b>0.4566</b>	0.2524	0.6353	<b>0.0908</b>	8.0699	0.9023	<b>0.4391</b>

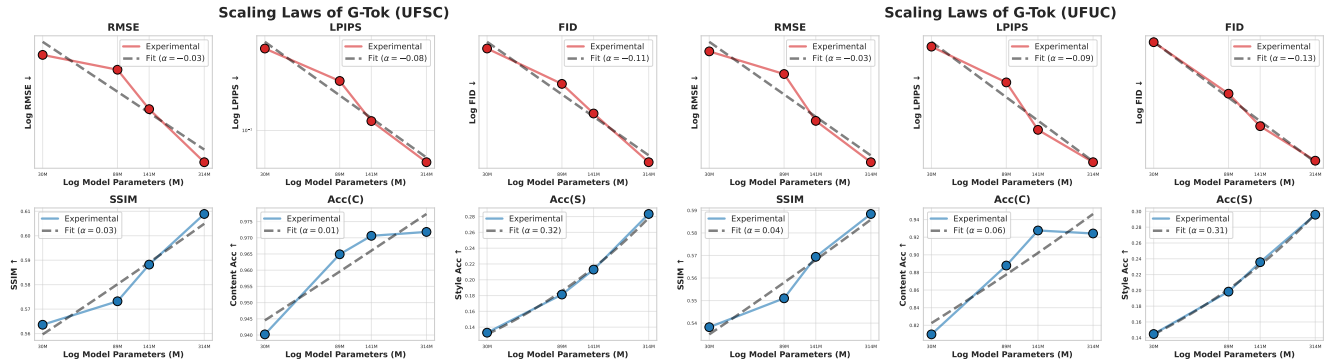


Figure S3. Scaling laws of the GAR-Font ( $I_8$ ) generator with NFA-128 and SE refinement. The plots show performance metrics across model sizes (30M, 89M, 141M, 314M) on Unseen Fonts Seen Characters (UFSC) and Unseen Fonts Unseen Characters (UFUC). The dashed lines represent power-law fits, highlighting the predictable improvements in both perceptual quality and style generalization.

Table S6. Quantitative evaluation of G-Tok’s architecture on Unseen Fonts. All models listed are pre-trained on the Small dataset.

Method	Unseen Fonts Seen Characters (UFSC)						Unseen Fonts Unseen Characters (UFUC)					
	RMSE↓	SSIM↑	LPIPS↓	FID↓	Acc(C)↑	Acc(S)↑	RMSE↓	SSIM↑	LPIPS↓	FID↓	Acc(C)↑	Acc(S)↑
CNN	0.3212	0.4836	0.1442	9.5071	0.9051	0.0235	0.3447	0.4350	0.1728	10.5239	0.6722	0.0221
CNN+Non-Causal ViT	0.3183	0.4919	0.1458	<b>7.9101</b>	0.9268	0.0402	0.3271	0.4745	0.1562	8.7504	0.8019	0.0436
CNN+Causal ViT	<b>0.3080</b>	<b>0.5052</b>	<b>0.1313</b>	7.9484	<b>0.9408</b>	<b>0.0802</b>	<b>0.3142</b>	<b>0.4932</b>	<b>0.1421</b>	<b>8.4841</b>	<b>0.8993</b>	<b>0.0796</b>

## D.5. Scaling Laws of GAR-Font( $I_8$ )

We evaluate the scalability of GAR-Font( $I_8$ ) with NFA-128 and SE on the small dataset by training models from 30M to 314M parameters and measuring performance across standard quantitative metrics. Following established scaling-law formulations, we model the relationship between model size  $N$  and loss metric  $L$  using a power law  $L(N) \propto N^{-\alpha}$ , and analyze trends in log–log space, where an ideal scaling law appears linear and the slope  $\alpha$  reflects scaling efficiency.

As shown in Fig. S3, the enhanced GAR-Font models closely follow these power-law predictions, exhibiting smooth, monotonic improvements across all metrics. Loss-based metrics (FID↓, LPIPS↓, RMSE↓) scale linearly with negative slopes, with FID↓ showing a pronounced gain, indicating that larger models continue to yield substantial perceptual improvements without saturation. Accuracy metrics display complementary behavior: Content Accuracy

(Acc(C)↑) saturates early due to task simplicity, whereas Style Accuracy (Acc(S)↑) benefits most from increased capacity. This steep scaling trend highlights that NFA and SE effectively exploit larger parameter budgets to capture and generalize complex stylistic attributes, underscoring the central role of scale in high-fidelity font generation.

## E. Additional Ablative Studies

### E.1. On G-Tok’s hybrid Architecture

To further illustrate the robustness of our hybrid CNN–ViT tokenizer, we provide complete visualizations of the **Reconstruction Robustness** experiment, where glyphs are corrupted with localized Gaussian noise ( $\sigma = 0.2$ , affecting 20% area). The qualitative results in Fig. S4 demonstrate that G-Tok robustly recovers structural layout and stylistic traits even under severe perturbations, while non-hybrid alternatives fail to reconstruct consistent structure.

Noisy Input	壹	恙	娃	壹	瞭	柞	轩	裾	喟	呛
CNN	壹	恙	娃	壹	瞭	柞	轩	裾	喟	呛
ViT-6	壹	恙	娃	壹	瞭	柞	轩	裾	喟	呛
CNN-ViT-6	壹	恙	娃	壹	瞭	柞	轩	裾	喟	呛
Target	壹	恙	娃	壹	瞭	柞	轩	裾	喟	呛

Figure S4. Reconstruction Robustness under localized Gaussian noise ( $\sigma = 0.2$ , 20% area).  $\square$  marks structural errors. G-Tok (CNN-ViT-6) preserves structure and style despite heavy corruption, while non-hybrid tokenizers exhibit unstable reconstructions.

## E.2. On G-Tok’s Global and Causal Modeling

We present full ablation results for the global and causal modeling components of G-Tok. Tab. S6 reports the complete quantitative comparison on the *UFSC/UFUC*. As discussed in Section 4.5.2, adding global self-attention (CNN + Non-causal ViT) significantly outperforms the CNN-only baseline, while the causal ViT further improves sequential modeling and yields the best overall performance.

Fig. S5 provides qualitative comparisons on (*UFSC*, Small) and (*UFUC*, Small). The AR Generator implemented with a CNN-only tokenizer often exhibits style mismatches and inconsistent strokes. Introducing ViT modules into the tokenizer enhances its ability to perceive and capture global stylistic context, leading to more coherent font generation. The AR variant with full G-Tok (CNN + Causal ViT) achieves the most robust performance, showing visible improvements in stylistic and structural fidelity.

## E.3. On AR Generator’s Soft-Decoding

We provide full visualizations to assess the impact of pixel-level supervision and the soft-decoding strategy. As shown in Fig. S6 under both (*UFSC*, Small) and (*UFUC*, Small), pixel-level supervision enhances structural accuracy, while soft decoding yields smoother, more continuous strokes and reduces broken segments and visual artifacts.

## E.4. On Multimodal Style Encoder’s Adaptation

We compare our decoupled multimodal training paradigm against joint training of the multimodal style encoder. While quantitative results are provided in Section 4.5.4, we present the full set of qualitative comparisons here.

Fig. S7 presents visual comparisons on (*UFSC/UFUC*, Large). The results reveal that GAR-Font( $M_2/M_4$ ), trained with the decoupled training scheme, generate glyphs whose font styles more closely align with the target compared to the jointly trained GAR-Font( $VL_2/VL_4$ ). They also demonstrate better character-structure accuracy. The decoupled training strategy enables the model to fully leverage the visual encoder’s representational capacity, thereby preserving fine-grained style features and structural priors that may be harder to retain under joint optimization.

## F. Visualization Results

### F.1. Comparison on Few-shot Font Generation

We provide complete visualizations for the experiment in Section 4.3. In Fig. S8, we show the full qualitative comparisons of visual-only FFG models trained on Small and Large datasets, evaluated under both *UFSC* and *UFUC* protocols. These results indicate that methods such as LF-Font, VQ-Font, DG-Font, CF-Font and Diff-Font often fail to preserve structural fidelity in intricate fonts. IF-Font tends to produce incomplete characters, while Font-Diffuser generates with inaccurate stroke widths. In contrast, GAR-Font( $I_8$ ,+NFA-8+SE) achieves the best style fidelity while maintaining structural consistency, effectively capturing fine stroke details of the target fonts.

### F.2. Efficient Vision-Language Adaptation

#### F.2.1. Pretrain

We provide full qualitative results complementing the experiment in Section 4.4. In Fig. S9, we show multimodal FFG comparisons under both *UFSC* and *UFUC* settings on the Large dataset, illustrating the improvements introduced by incorporating textual style descriptions in GAR-Font( $M_2$ ) and GAR-Font( $M_4$ ) compared with their vision-only counterparts. With textual style guidance, GAR-Font( $M_2$ ) and GAR-Font( $M_4$ ) better align with the target style, generating glyphs with strokes closely matching the target and improved structural fidelity.

#### F.2.2. Post-Refinement

To further assess the potential of our efficient vision-language adaptation, we apply the complete post-refinement pipeline (NFA-128 and SE) to GAR-Font( $M_2$ ) and GAR-Font( $M_4$ ). Fig. S10 presents qualitative results under *UFSC* and *UFUC* on the Large dataset. Applying NFA and SE post-refinement significantly improves both structural and style fidelity for all models. Textual guidance further enables GAR-Font( $M_2$ ) and GAR-Font( $M_4$ ) to more accurately capture the target style, yielding glyphs with improved style fidelity.

### F.3. Effect of Post-Refinement

To further analyze the effect of the post-refinement, we provide visual comparisons. As shown in Fig. S11, the pretrained GAR-Font( $I_8$ ) already produces characters with generally correct structures and styles, though minor font inconsistency exists. Applying NFA significantly improves style fidelity but may introduce slight distortions in fine strokes. The SE stage preserves style fidelity while further enhancing visual clarity and the accuracy of stroke details especially in complex fonts.

Content	许	验	摇	由	娱	仟	亿	苙	狎	舛	刹	纬	肖	追	僖	裳	展	七	涿	琛	琛	盆	叛	喷	漂	敲
CNN	许	验	摇	由	娱	仟	亿	苙	狎	舛	刹	纬	肖	追	僖	裳	展	七	涿	琛	琛	盆	叛	喷	漂	敲
CNN (+Non-Causal ViT)	许	验	摇	由	娱	仟	亿	苙	狎	舛	刹	纬	肖	追	僖	裳	展	七	涿	琛	琛	盆	叛	喷	漂	敲
CNN (+Causal ViT)	许	验	摇	由	娱	仟	亿	苙	狎	舛	刹	纬	肖	追	僖	裳	展	七	涿	琛	琛	盆	叛	喷	漂	敲
Target	许	验	摇	由	娱	仟	亿	苙	狎	舛	刹	纬	肖	追	僖	裳	展	七	涿	琛	琛	盆	叛	喷	漂	敲

(a) UFSC, Small dataset

Content	蚌	蝉	什	轩	伉	航	胞	掉	价	恰	绚	诊	肘	尙	跻	检	浇	狡	踞	浚	持	妨	格	绩	诃
CNN	蚌	蝉	什	轩	伉	航	胞	掉	价	恰	绚	诊	肘	尙	跻	检	浇	狡	踞	浚	持	妨	格	绩	诃
CNN (+Non-Causal ViT)	蚌	蝉	什	轩	伉	航	胞	掉	价	恰	绚	诊	肘	尙	跻	检	浇	狡	踞	浚	持	妨	格	绩	诃
CNN (+Causal ViT)	蚌	蝉	什	轩	伉	航	胞	掉	价	恰	绚	诊	肘	尙	跻	检	浇	狡	踞	浚	持	妨	格	绩	诃
Target	蚌	蝉	什	轩	伉	航	胞	掉	价	恰	绚	诊	肘	尙	跻	检	浇	狡	踞	浚	持	妨	格	绩	诃

(b) UFUC, Small dataset

Figure S5. Qualitative results on G-Tok's Global and Causal Modeling under UFSC and UFUC protocols (Small dataset).   /   indicate structural errors and style mismatches.

Content	赵	澈	舛	吟	颌	恒	柯	认	验	诒	菌	昞	盟	蛭	蹶	狎	獬	甑	懋	鸮	事	僖	蕃	蛄	螯
w/o pixel loss +hard decoding	赵	澈	舛	吟	颌	恒	柯	认	验	诒	菌	昞	盟	蛭	蹶	狎	獬	甑	懋	鸮	事	僖	蕃	蛄	螯
w/o pixel loss +soft decoding	赵	澈	舛	吟	颌	恒	柯	认	验	诒	菌	昞	盟	蛭	蹶	狎	獬	甑	懋	鸮	事	僖	蕃	蛄	螯
w/ pixel loss +hard decoding	赵	澈	舛	吟	颌	恒	柯	认	验	诒	菌	昞	盟	蛭	蹶	狎	獬	甑	懋	鸮	事	僖	蕃	蛄	螯
w/ pixel loss +soft decoding	赵	澈	舛	吟	颌	恒	柯	认	验	诒	菌	昞	盟	蛭	蹶	狎	獬	甑	懋	鸮	事	僖	蕃	蛄	螯
Target	赵	澈	舛	吟	颌	恒	柯	认	验	诒	菌	昞	盟	蛭	蹶	狎	獬	甑	懋	鸮	事	僖	蕃	蛄	螯

(a) UFSC, Small dataset

Content	叮	铬	哇	友	蝶	碍	跪	酪	膛	睢	咳	怜	拓	軼	轳	稗	侈	盼	挽	误	措	吭	尤	槎	锃
w/o pixel loss +hard decoding	叮	铬	哇	友	蝶	碍	跪	酪	膛	睢	咳	怜	拓	軼	轳	稗	侈	盼	挽	误	措	吭	尤	槎	锃
w/o pixel loss +soft decoding	叮	铬	哇	友	蝶	碍	跪	酪	膛	睢	咳	怜	拓	軼	轳	稗	侈	盼	挽	误	措	吭	尤	槎	锃
w/ pixel loss +hard decoding	叮	铬	哇	友	蝶	碍	跪	酪	膛	睢	咳	怜	拓	軼	轳	稗	侈	盼	挽	误	措	吭	尤	槎	锃
w/ pixel loss +soft decoding	叮	铬	哇	友	蝶	碍	跪	酪	膛	睢	咳	怜	拓	軼	轳	稗	侈	盼	挽	误	措	吭	尤	槎	锃
Target	叮	铬	哇	友	蝶	碍	跪	酪	膛	睢	咳	怜	拓	軼	轳	稗	侈	盼	挽	误	措	吭	尤	槎	锃

(b) UFUC, Small dataset

Figure S6. Qualitative results on AR Generator's Soft-decoding under UFSC and UFUC protocols (Small dataset).   /   indicate structural errors and style mismatches.

Content	洗	钹	聒	蹶	鲛	背	侧	担	借	溃	圮	蕃	唳	茆	忤	扒	耽	顷	冗	亿	举	纬	诱	涨	苙
GAR-Font(VL <sub>2</sub> )	洗	钹	聒	蹶	鲛	背	侧	担	借	溃	圮	蕃	唳	茆	忤	扒	耽	顷	冗	亿	举	纬	诱	涨	苙
GAR-Font(VL <sub>4</sub> )	洗	钹	聒	蹶	鲛	背	侧	担	借	溃	圮	蕃	唳	茆	忤	扒	耽	顷	冗	亿	举	纬	诱	涨	苙
GAR-Font(M <sub>2</sub> )	洗	钹	聒	蹶	鲛	背	侧	担	借	溃	圮	蕃	唳	茆	忤	扒	耽	顷	冗	亿	举	纬	诱	涨	苙
GAR-Font(M <sub>4</sub> )	洗	钹	聒	蹶	鲛	背	侧	担	借	溃	圮	蕃	唳	茆	忤	扒	耽	顷	冗	亿	举	纬	诱	涨	苙
Target	洗	钹	聒	蹶	鲛	背	侧	担	借	溃	圮	蕃	唳	茆	忤	扒	耽	顷	冗	亿	举	纬	诱	涨	苙

(a) UFSC, Large dataset

Content	根	角	拧	又	玎	胞	酷	挽	诅	鱿	呕	娃	佝	荃	屺	赐	怜	矣	兼	眯	瞥	嗜	纓	獾	蝥
GAR-Font(VL <sub>2</sub> )	根	角	拧	又	玎	胞	酷	挽	诅	鱿	呕	娃	佝	荃	屺	赐	怜	矣	兼	眯	瞥	嗜	纓	獾	蝥
GAR-Font(VL <sub>4</sub> )	根	角	拧	又	玎	胞	酷	挽	诅	鱿	呕	娃	佝	荃	屺	赐	怜	矣	兼	眯	瞥	嗜	纓	獾	蝥
GAR-Font(M <sub>2</sub> )	根	角	拧	又	玎	胞	酷	挽	诅	鱿	呕	娃	佝	荃	屺	赐	怜	矣	兼	眯	瞥	嗜	纓	獾	蝥
GAR-Font(M <sub>4</sub> )	根	角	拧	又	玎	胞	酷	挽	诅	鱿	呕	娃	佝	荃	屺	赐	怜	矣	兼	眯	瞥	嗜	纓	獾	蝥
Target	根	角	拧	又	玎	胞	酷	挽	诅	鱿	呕	娃	佝	荃	屺	赐	怜	矣	兼	眯	瞥	嗜	纓	獾	蝥

(b) UFUC, Large dataset

Figure S7. Qualitative results on Multimodal Style Encoder's Adaptation under UFSC and UFUC protocols (Large dataset).   /   indicate structural errors and style mismatches.

Content	侧	杆	韭	胯	枋	讽	否	焦	渍	抵	炊	瑰	勿	僂	弭	火	约	缥	眈	骹	倨	盔	霖	陆	疴
LF-Font	侧	杆	韭	胯	枋	讽	否	焦	渍	抵	炊	瑰	勿	僂	弭	火	约	缥	眈	骹	倨	盔	霖	陆	疴
VQ-Font	侧	杆	韭	胯	枋	讽	否	焦	渍	抵	炊	瑰	勿	僂	弭	火	约	缥	眈	骹	倨	盔	霖	陆	疴
DG-Font	侧	杆	韭	胯	枋	讽	否	焦	渍	抵	炊	瑰	勿	僂	弭	火	约	缥	眈	骹	倨	盔	霖	陆	疴
CF-Font	侧	杆	韭	胯	枋	讽	否	焦	渍	抵	炊	瑰	勿	僂	弭	火	约	缥	眈	骹	倨	盔	霖	陆	疴
IF-Font	侧	杆	韭	胯	枋	讽	否	焦	渍	抵	炊	瑰	勿	僂	弭	火	约	缥	眈	骹	倨	盔	霖	陆	疴
Diff-Font	侧	杆	韭	胯	枋	讽	否	焦	渍	抵	炊	瑰	勿	僂	弭	火	约	缥	眈	骹	倨	盔	霖	陆	疴
Font-Diffuser	侧	杆	韭	胯	枋	讽	否	焦	渍	抵	炊	瑰	勿	僂	弭	火	约	缥	眈	骹	倨	盔	霖	陆	疴
GAR-Font ( $I_b$ , +NFA-8+SE)	侧	杆	韭	胯	枋	讽	否	焦	渍	抵	炊	瑰	勿	僂	弭	火	约	缥	眈	骹	倨	盔	霖	陆	疴
Target	侧	杆	韭	胯	枋	讽	否	焦	渍	抵	炊	瑰	勿	僂	弭	火	约	缥	眈	骹	倨	盔	霖	陆	疴

(a) UFSC, Small dataset

Content	跟	歧	俗	宗	耐	稍	绍	渥	媛	倦	酪	峭	榆	孛	蹠	煌	炯	碰	谗	蝎	持	娃	坝	转	鲟
LF-Font	跟	歧	俗	宗	耐	稍	绍	渥	媛	倦	酪	峭	榆	孛	蹠	煌	炯	碰	谗	蝎	持	娃	坝	转	鲟
VQ-Font	跟	歧	俗	宗	耐	稍	绍	渥	媛	倦	酪	峭	榆	孛	蹠	煌	炯	碰	谗	蝎	持	娃	坝	转	鲟
DG-Font	跟	歧	俗	宗	耐	稍	绍	渥	媛	倦	酪	峭	榆	孛	蹠	煌	炯	碰	谗	蝎	持	娃	坝	转	鲟
CF-Font	跟	歧	俗	宗	耐	稍	绍	渥	媛	倦	酪	峭	榆	孛	蹠	煌	炯	碰	谗	蝎	持	娃	坝	转	鲟
IF-Font	跟	歧	俗	宗	耐	稍	绍	渥	媛	倦	酪	峭	榆	孛	蹠	煌	炯	碰	谗	蝎	持	娃	坝	转	鲟
Font-Diffuser	跟	歧	俗	宗	耐	稍	绍	渥	媛	倦	酪	峭	榆	孛	蹠	煌	炯	碰	谗	蝎	持	娃	坝	转	鲟
GAR-Font ( $I_b$ , +NFA-8+SE)	跟	歧	俗	宗	耐	稍	绍	渥	媛	倦	酪	峭	榆	孛	蹠	煌	炯	碰	谗	蝎	持	娃	坝	转	鲟
Target	跟	歧	俗	宗	耐	稍	绍	渥	媛	倦	酪	峭	榆	孛	蹠	煌	炯	碰	谗	蝎	持	娃	坝	转	鲟

(b) UFUC, Small dataset

Content	抱	测	凋	诹	洲	毗	漂	染	裳	挞	啊	侧	婚	舰	栗	激	襟	陆	律	么	阿	扒	雏	当	杂
LF-Font	抱	测	凋	诹	洲	毗	漂	染	裳	挞	啊	侧	婚	舰	栗	激	襟	陆	律	么	阿	扒	雏	当	杂
VQ-Font	抱	测	凋	诹	洲	毗	漂	染	裳	挞	啊	侧	婚	舰	栗	激	襟	陆	律	么	阿	扒	雏	当	杂
DG-Font	抱	测	凋	诹	洲	毗	漂	染	裳	挞	啊	侧	婚	舰	栗	激	襟	陆	律	么	阿	扒	雏	当	杂
CF-Font	抱	测	凋	诹	洲	毗	漂	染	裳	挞	啊	侧	婚	舰	栗	激	襟	陆	律	么	阿	扒	雏	当	杂
IF-Font	抱	测	凋	诹	洲	毗	漂	染	裳	挞	啊	侧	婚	舰	栗	激	襟	陆	律	么	阿	扒	雏	当	杂
Diff-Font	抱	测	凋	诹	洲	毗	漂	染	裳	挞	啊	侧	婚	舰	栗	激	襟	陆	律	么	阿	扒	雏	当	杂
Font-Diffuser	抱	测	凋	诹	洲	毗	漂	染	裳	挞	啊	侧	婚	舰	栗	激	襟	陆	律	么	阿	扒	雏	当	杂
GAR-Font ( $I_b$ , +NFA-8+SE)	抱	测	凋	诹	洲	毗	漂	染	裳	挞	啊	侧	婚	舰	栗	激	襟	陆	律	么	阿	扒	雏	当	杂
Target	抱	测	凋	诹	洲	毗	漂	染	裳	挞	啊	侧	婚	舰	栗	激	襟	陆	律	么	阿	扒	雏	当	杂

(c) UFSC, Large dataset

Content	宝	份	汉	价	泞	诚	埂	航	虻	襞	睬	灿	伺	樟	奕	踞	楷	酷	羌	蹋	猖	词	跟	科	洛
LF-Font	宝	份	汉	价	泞	诚	埂	航	虻	襞	睬	灿	伺	樟	奕	踞	楷	酷	羌	蹋	猖	词	跟	科	洛
VQ-Font	宝	份	汉	价	泞	诚	埂	航	虻	襞	睬	灿	伺	樟	奕	踞	楷	酷	羌	蹋	猖	词	跟	科	洛
DG-Font	宝	份	汉	价	泞	诚	埂	航	虻	襞	睬	灿	伺	樟	奕	踞	楷	酷	羌	蹋	猖	词	跟	科	洛
CF-Font	宝	份	汉	价	泞	诚	埂	航	虻	襞	睬	灿	伺	樟	奕	踞	楷	酷	羌	蹋	猖	词	跟	科	洛
IF-Font	宝	份	汉	价	泞	诚	埂	航	虻	襞	睬	灿	伺	樟	奕	踞	楷	酷	羌	蹋	猖	词	跟	科	洛
Font-Diffuser	宝	份	汉	价	泞	诚	埂	航	虻	襞	睬	灿	伺	樟	奕	踞	楷	酷	羌	蹋	猖	词	跟	科	洛
GAR-Font ( $I_b$ , +NFA-8+SE)	宝	份	汉	价	泞	诚	埂	航	虻	襞	睬	灿	伺	樟	奕	踞	楷	酷	羌	蹋	猖	词	跟	科	洛
Target	宝	份	汉	价	泞	诚	埂	航	虻	襞	睬	灿	伺	樟	奕	踞	楷	酷	羌	蹋	猖	词	跟	科	洛

(d) UFUC, Large dataset

Figure S8. Qualitative results on vision-only FFG across UFSC/UFUC protocols and Small/Large datasets.   /   indicate structural errors and style mismatches.

Content	诨	柳	吟	桢	钹	耗	欺	清	吟	铙	尽	瑞	倘	醒	茁	遍	订	钩	坞	弭	之	諏	驥	豕	整
$n_{ref} = 2$	诨	柳	吟	桢	钹	耗	欺	清	吟	铙	尽	瑞	倘	醒	茁	遍	订	钩	坞	弭	之	諏	驥	豕	整
$n_{ref} = 4$	诨	柳	吟	桢	钹	耗	欺	清	吟	铙	尽	瑞	倘	醒	茁	遍	订	钩	坞	弭	之	諏	驥	豕	整
$n_{ref} = 8$	诨	柳	吟	桢	钹	耗	欺	清	吟	铙	尽	瑞	倘	醒	茁	遍	订	钩	坞	弭	之	諏	驥	豕	整
Textual style description	"A font that exhibits sharp strokes and angular rhythm, conveying energy and tension."					"A font that features smooth curves and gentle flow, evoking warmth and elegance."					"A font that combines graceful brush rhythm with open spacing, expressing a calm and refined charm."					"A font that blends dynamic brushwork with balanced structure, showing lively yet stable form."					"A font that presents bold, square strokes and solid geometry, reflecting order and strength."				
GAR-Font( $M_2$ )	诨	柳	吟	桢	钹	耗	欺	清	吟	铙	尽	瑞	倘	醒	茁	遍	订	钩	坞	弭	之	諏	驥	豕	整
GAR-Font( $M_4$ )	诨	柳	吟	桢	钹	耗	欺	清	吟	铙	尽	瑞	倘	醒	茁	遍	订	钩	坞	弭	之	諏	驥	豕	整
Target	诨	柳	吟	桢	钹	耗	欺	清	吟	铙	尽	瑞	倘	醒	茁	遍	订	钩	坞	弭	之	諏	驥	豕	整

(a) UFSC, Large dataset

Content	格	沮	喟	驿	鲟	角	起	伦	焦	薪	蜗	误	沾	捍	悝	纯	罗	木	扬	狻	努	什	渥	槿	睇
$n_{ref} = 2$	格	沮	喟	驿	鲟	角	起	伦	焦	薪	蜗	误	沾	捍	悝	纯	罗	木	扬	狻	努	什	渥	槿	睇
$n_{ref} = 4$	格	沮	喟	驿	鲟	角	起	伦	焦	薪	蜗	误	沾	捍	悝	纯	罗	木	扬	狻	努	什	渥	槿	睇
$n_{ref} = 8$	格	沮	喟	驿	鲟	角	起	伦	焦	薪	蜗	误	沾	捍	悝	纯	罗	木	扬	狻	努	什	渥	槿	睇
Textual style description	"A font that carries loose, flowing strokes, conveying spontaneity and free-form charm."					"A font that presents neat, graceful lines, offering clarity and traditional elegance."					"A font that displays bold, cursive motion, expressing sweeping energy and vivid dynamism."					"A font that features soft, rounded shapes, evoking playfulness and cheerful warmth."					"A font that adopts dense, structured strokes, projecting strength and solidity."				
GAR-Font( $M_2$ )	格	沮	喟	驿	鲟	角	起	伦	焦	薪	蜗	误	沾	捍	悝	纯	罗	木	扬	狻	努	什	渥	槿	睇
GAR-Font( $M_4$ )	格	沮	喟	驿	鲟	角	起	伦	焦	薪	蜗	误	沾	捍	悝	纯	罗	木	扬	狻	努	什	渥	槿	睇
Target	格	沮	喟	驿	鲟	角	起	伦	焦	薪	蜗	误	沾	捍	悝	纯	罗	木	扬	狻	努	什	渥	槿	睇

(b) UFUC, Large dataset

Figure S9. Qualitative results of Pre-Train multimodal FFG under UFSC and UFUC protocols (Large dataset).  denotes local slight structural mistakes, and  marks stylistic drift.

Content	臂	答	傅	柜	椅	返	焦	抛	赦	垓	阿	不	氮	激	砸	芬	否	盍	奇	尧	溃	迷	添	湾	汕
$n_{ref} = 2$	臂	答	傅	柜	椅	返	焦	抛	赦	垓	阿	不	氮	激	砸	芬	否	盍	奇	尧	溃	迷	添	湾	汕
$n_{ref} = 4$	臂	答	傅	柜	椅	返	焦	抛	赦	垓	阿	不	氮	激	砸	芬	否	盍	奇	尧	溃	迷	添	湾	汕
$n_{ref} = 8$	臂	答	傅	柜	椅	返	焦	抛	赦	垓	阿	不	氮	激	砸	芬	否	盍	奇	尧	溃	迷	添	湾	汕
Textual style description	"A font that shows neat strokes and clear structure, delivering a neat and orderly vibe."					"A font that features strong presence, conveying a bold and striking impression."					"A font that has lively strokes and flexible shapes, expressing a vivid and casual charm."					"A font that presents bold strokes and rounded corners, showing a cute and solid style."					"A font that carries gentle lines and soft texture, bringing a warm and approachable feel."				
GAR-Font( $M_2$ )	臂	答	傅	柜	椅	返	焦	抛	赦	垓	阿	不	氮	激	砸	芬	否	盍	奇	尧	溃	迷	添	湾	汕
GAR-Font( $M_4$ )	臂	答	傅	柜	椅	返	焦	抛	赦	垓	阿	不	氮	激	砸	芬	否	盍	奇	尧	溃	迷	添	湾	汕
Target	臂	答	傅	柜	椅	返	焦	抛	赦	垓	阿	不	氮	激	砸	芬	否	盍	奇	尧	溃	迷	添	湾	汕

(a) UFSC, Large dataset

Content	竿	硅	阶	扣	温	螺	馒	秒	偏	绍	表	埂	龙	七	绪	饯	距	虑	起	嗜	琼	惚	睇	婢	跣
$n_{ref} = 2$	竿	硅	阶	扣	温	螺	馒	秒	偏	绍	表	埂	龙	七	绪	饯	距	虑	起	嗜	琼	惚	睇	婢	跣
$n_{ref} = 4$	竿	硅	阶	扣	温	螺	馒	秒	偏	绍	表	埂	龙	七	绪	饯	距	虑	起	嗜	琼	惚	睇	婢	跣
$n_{ref} = 8$	竿	硅	阶	扣	温	螺	馒	秒	偏	绍	表	埂	龙	七	绪	饯	距	虑	起	嗜	琼	惚	睇	婢	跣
Textual style description	"A font that displays chiselled strokes, evoking a bold texture with spirited tension."					"A font that carries loose, swaying brush motion, suggesting casual elegance and expressive fluidity."					"A font that emphasizes firm, weighty structure, conveying stability with a strong presence."					"A font that shows rounded bold contours, creating a friendly fullness with confident impact."					"A font that blends thick, lively strokes with playful exaggeration, evoking charm and energy."				
GAR-Font( $M_2$ )	竿	硅	阶	扣	温	螺	馒	秒	偏	绍	表	埂	龙	七	绪	饯	距	虑	起	嗜	琼	惚	睇	婢	跣
GAR-Font( $M_4$ )	竿	硅	阶	扣	温	螺	馒	秒	偏	绍	表	埂	龙	七	绪	饯	距	虑	起	嗜	琼	惚	睇	婢	跣
Target	竿	硅	阶	扣	温	螺	馒	秒	偏	绍	表	埂	龙	七	绪	饯	距	虑	起	嗜	琼	惚	睇	婢	跣

(b) UFUC, Large dataset

Figure S10. Qualitative results of Post-Refine multimodal FFG under UFSC and UFUC protocols (Large dataset).  denotes local slight structural mistakes, and  marks stylistic drift.



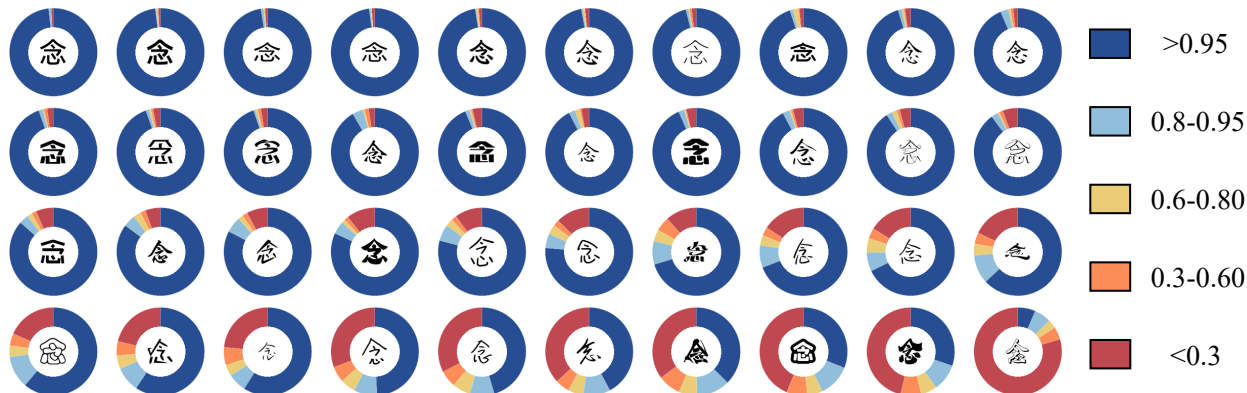


Figure S14. Content confidence distribution of GAR-Font generated characters across different font styles. Each pie chart corresponds to a specific font, indicated by the central character. The color segments represent the proportion of samples falling into different content confidence ranges, highlighting that more complex styles tend to have lower content confidence.



Figure S15. Failure cases.   highlights regions with dense details where GAR-Font tends to produce distorted strokes.

#### F.4. Cross-Language Font Synthesis

To evaluate the generalizability of GAR-Font, we conduct a cross-language experiment in which the model synthesizes Korean characters using styles learned from Chinese fonts. As shown in Fig. S12, GAR-Font accurately generates Korean characters while preserving the reference font style, demonstrating the effective generalization of our method.

#### F.5. High-Resolution Font Generation

To demonstrate the scalability of GAR-Font beyond the  $64 \times 64$  resolution adopted in our main experiments, we modify the CNN encoder within G-Tok to discretize a  $128 \times 128$  glyph into 64 tokens, corresponding to a downsample ratio of 16. As illustrated in Fig. S13, GAR-Font maintains both style faithfulness and structural fidelity at this increased resolution, demonstrating its potential in high-resolution font generation tasks.

#### F.6. More GAR-Font Generation Examples

To illustrate the capabilities of GAR-Font, we generate the full GB2312 character set for five test fonts with GAR-Font( $I_8$ , +NFA-8+SE, trained on Large dataset) and randomly select 1,280 samples per font. The generated glyphs are shown in Fig. S16-Fig. S20, demonstrating the model’s ability to produce large-scale character sets while faithfully preserving each font’s distinctive stylistic features.

### G. Failure Cases and Analysis

While GAR-Font generally performs well, distortions and blurring occasionally appear in dense-stroke regions of highly complex fonts (Fig. S15). To investigate this, we applied a content classifier to all *UFUC* samples generated by GAR-Font( $I_8$ ,+NFA-128+SE), using the softmax output as a measure of content confidence. The results reveal a clear trend: content confidence notably decreases as stylistic complexity increases (Fig. S14), suggesting the model sometimes sacrifices structural accuracy to better capture stylistic features.

We hypothesize that this structural degradation results from the error accumulation inherent in autoregressive modeling. Without explicit structural constraints, the model tends to drift when generating intricate stroke patterns. A promising direction for future work is to incorporate explicit structural priors, such as character skeletons or stroke sequences, to guide the generation process. This would help preserve structural fidelity in complex styles.



蚯角给只剪昂狐忱豫泽塘愕整淘遐莫险晖泐牌匈泸孕琦誓俑贬鹊凋蛄辄妨沁谓楚硝含视蛮渣  
氩析毛躯尤论镍吉排鯉因魏缸唐快帽盟露钆禀詹阮车钥冀捕湔私俐艾净暖干苻鹏剧展百逦轻囹  
叭鄢襦坳礴舵悲绢牯甸舌姻余形殒辘动遁怡七邛侏赜齿蟻仆衿艾净暖干苻鹏剧展百逦轻囹  
鲑普承睢橙检莠汴颠靡塘淇鼻亼迢竣引动遁怡七邛侏赜齿蟻仆衿艾净暖干苻鹏剧展百逦轻囹  
脐痘瑋洋锺桤窈胸位奎羈继徙怵琅谋铭讽终涪拍瘳翰多扮膂担咧孵瘰口桐鬣恃流沮沆柔咚纒  
毫领都筭三勒翊假藉径箩憾命苻幸旆鞭砣振遂矮汐辞晃钶馭廝匭匭匭匭匭匭匭匭匭匭匭匭匭匭  
入埃惨鬲镇闾躅膨颗搏姥拱聊泊猎忤肥帮振遂矮汐辞晃钶馭廝匭匭匭匭匭匭匭匭匭匭匭匭  
瘰去串臆离绩作宄绣恋己邗括殪首芝钉呢舛韭羊炆芭蛭郑铝汀柏攫才真吮檬橘榘符幕掀纳颞砗  
暖葭上绒曛雪桃犁略诶液尝埭氛封峒跖趾蝼蛄腥臍膂臍膂臍膂臍膂臍膂臍膂臍膂臍膂臍膂臍膂  
虺疤迓倦蛄头楷靠蓉喙洽畦婊氛封峒跖趾蝼蛄腥臍膂臍膂臍膂臍膂臍膂臍膂臍膂臍膂臍膂臍膂  
弧冉狮暨术状娃忌互誉氟精厨姨鸷束跪遣跛踬阍徊仉蕊郁嘈八巾芳屏淬炙公妞唅符幕掀纳颞砗  
彤米腕枕厘阐勿莖谣缥媒捨晋慵淮玲依朵站蜈培莩往驯邀诿汪殡蒂莩屏淬炙公妞唅符幕掀纳颞砗  
抉飙完辄芋褊婴某蚵蛟文恙宪淆秦筇鰓踢馘冯晤鲛匿睽淀皓袿僵窗针帙听速侣鸡芹荒园蒺聒听  
婧抵苙瑚虎疚魔耍合僧陞骼稀羸聆鳧鳧鳧鳧鳧鳧鳧鳧鳧鳧鳧鳧鳧鳧鳧鳧鳧鳧鳧鳧鳧鳧鳧鳧  
漱六室铤劈峨寄碎替亚脍膂肩筑道停隼隼隼隼隼隼隼隼隼隼隼隼隼隼隼隼隼隼隼隼隼隼隼隼  
蘧袄惋岖昱伊钧卡银墅瘠肩筑道停隼隼隼隼隼隼隼隼隼隼隼隼隼隼隼隼隼隼隼隼隼隼隼隼  
硷苓挑掇罩绿鸞塬初遛萨旨锦梯剑赚孝髦紊嘱槟痴姐痊恂恂恂恂恂恂恂恂恂恂恂恂恂恂恂恂恂  
璫但僭静欲幹循齧到桴尴克切扳受戴闾砗榘榘榘榘榘榘榘榘榘榘榘榘榘榘榘榘榘榘榘榘榘榘榘  
否癘嚙抡芟案垢磨椽隧词僇切扳受戴闾砗榘榘榘榘榘榘榘榘榘榘榘榘榘榘榘榘榘榘榘榘榘榘  
氨禹扩哀蕞腴稼域界鲫烬逢乏蹬球袂迭竖芭薇祥门音翔钱十曷摸街轿股钺敛赌琊指酷亮佛哺持莠  
溟木闯胝伙擗躅团荟火幄顾蒜啤划俸渡微淌橄运达溢耙弟恃硬裙歛眩眯樵葬抛笑蠢翩澹碍醅砗  
腋声馗恬桃蔗锺矸鹑噫刘缸徇蒜啤划俸渡微淌橄运达溢耙弟恃硬裙歛眩眯樵葬抛笑蠢翩澹碍醅砗  
呵悠骥咯仅泞捣嫫若慨璧洁间罗樟洛劾匆梢汁瑾榘榘榘榘榘榘榘榘榘榘榘榘榘榘榘榘榘榘榘榘  
靳捍糙另叮素龋茗慨璧洁间罗樟洛劾匆梢汁瑾榘榘榘榘榘榘榘榘榘榘榘榘榘榘榘榘榘榘榘榘  
岭鹁肋晒别联楸呗姑醇尔擗畴营戈交选廉答蝼寅啜贻付凉弥坛酥酥扬片钲饬饬饬饬饬饬饬饬  
淳孽绪洩滨霖枕钗无伺樨砗颖迹邠郇警驕踣踣踣踣踣踣踣踣踣踣踣踣踣踣踣踣踣踣踣踣踣踣踣  
壤哪琉狼阼叟骊钰居趋蠕锈贡悼郇警驕踣踣踣踣踣踣踣踣踣踣踣踣踣踣踣踣踣踣踣踣踣踣踣  
道味脸谦情芝藉源炊碇冷槩彩芭倨杓湿馨倥熙砂斜劬喙豸别然垓荏荏荏荏荏荏荏荏荏荏荏荏  
叩诽氩洪圳喷观穉枣敞媪澜偃氧羞子耄屁怯楼朱猷考黥豸别然垓荏荏荏荏荏荏荏荏荏荏荏荏  
邑賧於裆雉绩洽颇唾着其辱雯氧羞子耄屁怯楼朱猷考黥豸别然垓荏荏荏荏荏荏荏荏荏荏荏荏  
蜓屐僭扯縿逝箕才中咆抽犹您窃服到杪殊纒纒纒纒纒纒纒纒纒纒纒纒纒纒纒纒纒纒纒纒纒纒纒  
挺枷继绑萍双纲嘉捏鹤醅帛嫫饿煲玢鸫蹀昶伶阳琮堃挈枨橈狠各兼鯉盗抵怪式尺髭剪邓聳邵但

Figure S17. Generated glyphs from test fonts using GAR-Font( $I_8$ , +NFA-8+SE, Large dataset).

榆龔龔芳崦鹤盈碗党能责踞撑壕蛺蛺衾粥跼洁懂梢淡渫貌暖策鸱陌匀茨充猷隘燧燧  
 齿盐别鞍港畔淫憩日无蛤炷淤痧抽戴圻著绿趋鸨惶痴献矜悼算抡婆庠狙樨卓跟秣甜焙  
 黼斌知樵屿舍嗔碇圆酸柏迹踈炖白渲扬潞蔽舫耐窥篆帐篝窕总菩溟逐残熊郊崆呐潼堯  
 纲枋蟹现民忿阙喏构疼衿粗怙腮首预郝霖剋戮砍蚣疣眠刚紧叩僖串衬恰焯组滄巷焯  
 下木忙研慰象锚荊稀邾壁遣鲜锁惯资莩苑观点喷弹紇眩繁欠遣汹欧娇饕组滄巷焯  
 侗钢碗闷欬猱哄蛆波捺夸掩攘奠互宰烟卸妻妒桦鏗鰻淑付诸钶昂糯莩兜踣踣会陶泔  
 喘浩埂泪新盲滨槎甫冒忤葱管眉裘忠灰兰尖酊桡藜龄惧萨付诸钶昂糯莩兜踣踣会陶泔  
 两积别饕湄覆倦糗充蛞掣如瞥翻鞘啦分迈莩估变累铀宗迥榜昂糯莩兜踣踣会陶泔  
 吸那恫致破绘请依洵诘焚暗蔗环销访莩佳咤穗惶赠汽柯挪颀停乞递崇殒兼侈稳鄙迟所  
 带郑矜版巽揭赜称毫彳砗洙丢蕺佳滓邛湛绉拾塌浣幸归晤奎降重祈鑽痘榻桑拾辐妙伏  
 蹀蠕圩疆肪挺洳剡猷仆六铎黄沅役莩察贲由恣咆陈麻摆桃愤企枕庖醇罽楼蝉逼匀勤芭  
 罪衰糙捣靠灸久炫脚蹄榨首坭竹铎整樟菡蚶茎祖猴娄唯那欽惟庖醇罽楼蝉逼匀勤芭  
 夕霏铃商桦彘老芒瞎错门踏垦未育窈吝拒彩揆恍怕娃鲭掩檣僂狃连梯幄倭坏羊蹉颀吉  
 继惹脱嫫嫁核识慨绿悒浚倦炆俗爱鏊黠吮蚊岬美饨蔡岬邠嫌烦费咎铍初舫扼左旅璃钿  
 偌舍秉共朕端运匪晓濒甥眷钺那爱鏊黠吮蚊岬美饨蔡岬邠嫌烦费咎铍初舫扼左旅璃钿  
 倚慕懦史咯鸨鹄钺熙局迷邗件幸蹠豕冶梳帑媛渡札斫扩履烦费咎铍初舫扼左旅璃钿  
 诰佳里妩俐响隈善鸨钺熙局迷邗件幸蹠豕冶梳帑媛渡札斫扩履烦费咎铍初舫扼左旅璃钿  
 茎芦情蚯狷襄肆萌恻们斑钉碾哨愁怎磔妒晖般友礴任送植炒岂枵薰谿鸨纺坊絃戮蛆  
 异桀尹怀莨俳谲砸有源吟弩欵采雪悬驹汤愈蕨聘矜熟喙傀癩类茫幸乌衙娜菜涉祝邢  
 熹魏作漆葦爹慢得谪楸短悟菴璫情仙啼峒旗薪脍题溘盥京半夏笋愉丰恃坊渚藻樾哮  
 杪邗拙腕觞裕砒鎌笱谗羌格褐喧右缙辞柱峡啡葵厚排葦妖狩獬栖泊谖髭谋劣砚煨樾  
 咻着歧甬棟朱性璜虾祀煜刁幕儒漠岂嚙芬雍恙满狡竭磷逖嚙疏入桥晒宋魁韧轻渚耶  
 八教錮掎卉冀姍控妥鸨烟驥峭犹迎良瑚眩帆宦什醒凄恚纒软应啜罢钵嗅铈眯啗贖  
 位萱承铨殿伏越搜氛辱瘁媵皓菜跑嗜笔笋陔枳镊桥筒叭烙隰诈岸淙荏帜嘍漾碍泯耐  
 岷肘与椽尤璐铤钮茗负铈萑粒喇铉沽促鬲乙炮糟碳统菴荔溢深緌逐倪周份劭隧坝  
 祥神絳睛郢胝柰振执福襟渤遍齋飀彬田汗夷略奉揖迅掖榛黠乱恣耦捐炅棘萬用蛻  
 芳污腐碎泌诱貳柅萌寻璞挫骑赛缦谯齿噉绸荒再沔赬屋黝纒焯焯焯焯焯焯焯焯焯焯  
 散曩清纹模遥岫焯息现昔菴铅范縗缙免蠲脾顛恒派蹂噉矇矇矇矇矇矇矇矇矇矇矇矇  
 咄萧凶错淪桃奕暇拓醪埭蓄咋咙筛让护岐牟筮蹭撮窞径柎槽尸脐嵘髦缠蛛指唇枝坞  
 法陡措脑囤逮槎枫啼普熏擅欺圮褪停碍敦阿啜叫缙超息裾江岑伞戍保幢盟蛸啉宰果  
 悻来秩蒯歌楠幼心嫫黻溥读铈定孰榻岫嶷答枘夯高嫌遣雕茎縑沫桓想险谓惺侏縷遭涸

Figure S18. Generated glyphs from test fonts using GAR-Font( $I_8$ , +NFA-8+SE, Large dataset).





## References

- [1] Jean-Baptiste Alayrac, Jeff Donahue, Pauline Luc, Antoine Miech, Iain Barr, Yana Hasson, Karel Lenc, Arthur Mensch, Katherine Millican, Malcolm Reynolds, et al. Flamingo: a visual language model for few-shot learning. *Advances in neural information processing systems*, 35:23716–23736, 2022. 2, 3
- [2] Roman Bachmann, Jesse Allardice, David Mizrahi, Enrico Fini, Oğuzhan Fatih Kar, Elmira Amirloo, Alaaeldin El-Nouby, Amir Zamir, and Afshin Dehghan. Flextok: Resampling images into 1d token sequences of flexible length. In *Forty-second International Conference on Machine Learning*, 2025. 2
- [3] Shuai Bai, Keqin Chen, Xuejing Liu, Jialin Wang, Wenbin Ge, Sibao Song, Kai Dang, Peng Wang, Shijie Wang, Jun Tang, et al. Qwen2. 5-vl technical report. *arXiv preprint arXiv:2502.13923*, 2025. 6
- [4] Ankan Kumar Bhunia, Ayan Kumar Bhunia, Prithaj Banerjee, Aishik Konwer, Abir Bhowmick, Partha Pratim Roy, and Umapada Pal. Word level font-to-font image translation using convolutional recurrent generative adversarial networks. In *2018 24th International Conference on Pattern Recognition (ICPR)*, pages 3645–3650. IEEE, 2018. 2
- [5] Shiyue Cao, Yueqin Yin, Lianghua Huang, Yu Liu, Xin Zhao, Deli Zhao, and Kaigi Huang. Efficient-vqgan: Towards high-resolution image generation with efficient vision transformers. In *Proceedings of the IEEE/CVF International Conference on Computer Vision*, pages 7368–7377, 2023. 2
- [6] Siyu Cao, Hangting Chen, Peng Chen, Yiji Cheng, Yutao Cui, Xincheng Deng, Ying Dong, Kipper Gong, Tianpeng Gu, Xiuse Gu, et al. Hunyuanimage 3.0 technical report. *arXiv preprint arXiv:2509.23951*, 2025. 2
- [7] Yunkang Cao, Jiangning Zhang, Luca Frittoli, Yuqi Cheng, Weiming Shen, and Giacomo Boracchi. Adaclip: Adapting clip with hybrid learnable prompts for zero-shot anomaly detection. In *European Conference on Computer Vision*, pages 55–72. Springer, 2024. 3
- [8] Junbum Cha, Sanghyuk Chun, Gayoung Lee, Bado Lee, Seonghyeon Kim, and Hwalsuk Lee. Few-shot compositional font generation with dual memory. In *European conference on computer vision*, pages 735–751. Springer, 2020. 2
- [9] Bo Chang, Qiong Zhang, Shenyi Pan, and Lili Meng. Generating handwritten chinese characters using cyclegan. In *2018 IEEE winter conference on applications of computer vision (WACV)*, pages 199–207. IEEE, 2018. 2
- [10] Huiwen Chang, Han Zhang, Lu Jiang, Ce Liu, and William T Freeman. Maskgit: Masked generative image transformer. In *Proceedings of the IEEE/CVF conference on computer vision and pattern recognition*, pages 11315–11325, 2022. 2
- [11] Jie Chang, Yujun Gu, Ya Zhang, YanFeng Wang, and CM Innovation. Chinese handwriting imitation with hierarchical generative adversarial network. In *BMVC*, page 290, 2018. 2
- [12] Mark Chen, Alec Radford, Rewon Child, Jeffrey Wu, Heewoo Jun, David Luan, and Ilya Sutskever. Generative pre-training from pixels. In *International conference on machine learning*, pages 1691–1703. PMLR, 2020. 2
- [13] Xinping Chen, Xiao Ke, and Wenzhong Guo. If-font: Ideographic description sequence-following font generation. In *Advances in Neural Information Processing Systems*, pages 14177–14199. Curran Associates, Inc., 2024. 1, 5
- [14] Xiaokang Chen, Zhiyu Wu, Xingchao Liu, Zizheng Pan, Wen Liu, Zhenda Xie, Xingkai Yu, and Chong Ruan. Januspro: Unified multimodal understanding and generation with data and model scaling. *arXiv preprint arXiv:2501.17811*, 2025. 2
- [15] Chaorui Deng, Deyao Zhu, Kunchang Li, Chenhui Gou, Feng Li, Zeyu Wang, Shu Zhong, Weihao Yu, Xiaonan Nie, Ziang Song, et al. Emerging properties in unified multimodal pretraining. *arXiv preprint arXiv:2505.14683*, 2025. 2
- [16] Alexey Dosovitskiy, Lucas Beyer, Alexander Kolesnikov, Dirk Weissenborn, Xiaohua Zhai, Thomas Unterthiner, Mostafa Dehghani, Matthias Minderer, Georg Heigold, Sylvain Gelly, et al. An image is worth 16x16 words: Transformers for image recognition at scale. *arXiv preprint arXiv:2010.11929*, 2020. 3
- [17] Patrick Esser, Robin Rombach, and Bjorn Ommer. Taming transformers for high-resolution image synthesis. In *Proceedings of the IEEE/CVF conference on computer vision and pattern recognition*, pages 12873–12883, 2021. 2, 3
- [18] Bin Fu, Fanghua Yu, Anran Liu, Zixuan Wang, Jie Wen, Junjun He, and Yu Qiao. Generate like experts: multi-stage font generation by incorporating font transfer process into diffusion models. In *Proceedings of the IEEE/CVF conference on computer vision and pattern recognition*, pages 6892–6901, 2024. 2
- [19] Yue Gao, Yuan Guo, Zhouhui Lian, Yingmin Tang, and Jianguo Xiao. Artistic glyph image synthesis via one-stage few-shot learning. *ACM Transactions on Graphics (ToG)*, 38(6): 1–12, 2019. 2
- [20] Yuying Ge, Sijie Zhao, Jinguo Zhu, Yixiao Ge, Kun Yi, Lin Song, Chen Li, Xiaohan Ding, and Ying Shan. Seed-x: Multimodal models with unified multi-granularity comprehension and generation. *arXiv preprint arXiv:2404.14396*, 2024. 2
- [21] Haibin He, Xinyuan Chen, Chaoyue Wang, Juhua Liu, Bo Du, Dacheng Tao, and Qiao Yu. Diff-font: Diffusion model for robust one-shot font generation. *International Journal of Computer Vision*, 132(11):5372–5386, 2024. 1, 2, 5
- [22] Xiao He, Mingrui Zhu, Nannan Wang, and Xinbo Gao. Few-shot font generation by learning style difference and similarity. *IEEE Transactions on Circuits and Systems for Video Technology*, 34(9):8013–8025, 2024. 2
- [23] Edward J Hu, Yelong Shen, Phillip Wallis, Zeyuan Allen-Zhu, Yuanzhi Li, Shean Wang, Lu Wang, Weizhu Chen, et al. Lora: Low-rank adaptation of large language models. *ICLR*, 1(2):3, 2022. 3
- [24] Mengqi Huang, Zhendong Mao, Quan Wang, and Yongdong Zhang. Not all image regions matter: Masked vector quantization for autoregressive image generation. In *Proceedings of the IEEE/CVF Conference on Computer Vision and Pattern Recognition*, pages 2002–2011, 2023. 2

- [25] Yuanhui Huang, Weiliang Chen, Wenzhao Zheng, Yueqi Duan, Jie Zhou, and Jiwen Lu. Spectralar: Spectral autoregressive visual generation. In *Proceedings of the IEEE/CVF International Conference on Computer Vision*, pages 15842–15852, 2025. 1, 2
- [26] Zhihao Huang, Xi Qiu, Yukuo Ma, Yifu Zhou, Junjie Chen, Hongyuan Zhang, Chi Zhang, and Xuelong Li. Nfig: Autoregressive image generation with next-frequency prediction. *arXiv preprint arXiv:2503.07076*, 2025. 2
- [27] Yue Jiang, Zhouhui Lian, Yingmin Tang, and Jianguo Xiao. Scfont: Structure-guided chinese font generation via deep stacked networks. In *Proceedings of the AAAI conference on artificial intelligence*, pages 4015–4022, 2019. 2
- [28] Younghwi Kim, Seok Chan Jeong, and Sunghyun Sim. Legacy learning using few-shot font generation models for automatic text design in metaverse content: Cases studies in korean and chinese. *arXiv preprint arXiv:2408.16900*, 2024. 2
- [29] Yuxin Kong, Canjie Luo, Weihong Ma, Qiyuan Zhu, Sheng-gao Zhu, Nicholas Yuan, and Lianwen Jin. Look closer to supervise better: One-shot font generation via component-based discriminator. In *Proceedings of the IEEE/CVF conference on computer vision and pattern recognition*, pages 13482–13491, 2022. 1
- [30] Myungkyu Koo, Subin Kim, Sangkyung Kwak, Jaehyun Nam, Seojin Kim, and Jinwoo Shin. Fontadapter: Instant font adaptation in visual text generation. *arXiv preprint arXiv:2506.05843*, 2025. 3
- [31] Doyup Lee, Chiheon Kim, Saehoon Kim, Minsu Cho, and Wook-Shin Han. Autoregressive image generation using residual quantization. In *Proceedings of the IEEE/CVF conference on computer vision and pattern recognition*, pages 11523–11532, 2022. 2
- [32] Chunyuan Li, Cliff Wong, Sheng Zhang, Naoto Usuyama, Haotian Liu, Jianwei Yang, Tristan Naumann, Hoifung Poon, and Jianfeng Gao. Llava-med: Training a large language-and-vision assistant for biomedicine in one day. *Advances in Neural Information Processing Systems*, 36:28541–28564, 2023. 2
- [33] Hua Li and Zhouhui Lian. Ffh-font: few-shot chinese font synthesis with higher quality, faster speed, and higher resolution. *ACM Transactions on Graphics (TOG)*, 43(6):1–16, 2024. 1, 2, 5
- [34] Shilin Li and Anna Zhu. Fstdiff: One-shot font generation via cross-font style transformation learning. In *International Conference on Document Analysis and Recognition*, pages 167–182. Springer, 2025. 2
- [35] Xiang Li, Kai Qiu, Hao Chen, Jason Kuen, Jiuxiang Gu, Bhiksha Raj, and Zhe Lin. Imagefolder: Autoregressive image generation with folded tokens. *arXiv preprint arXiv:2410.01756*, 2024. 2
- [36] Zhouhui Lian and Yichen Gao. Cvfont: Synthesizing chinese vector fonts via deep layout inferring. In *Computer Graphics Forum*, pages 212–225. Wiley Online Library, 2022. 2
- [37] Zhouhui Lian, Bo Zhao, Xudong Chen, and Jianguo Xiao. Easyfont: a style learning-based system to easily build your large-scale handwriting fonts. *ACM Transactions on Graphics (TOG)*, 38(1):1–18, 2018. 2
- [38] Bin Lin, Yang Ye, Bin Zhu, Jiayi Cui, Munan Ning, Peng Jin, and Li Yuan. Video-llava: Learning united visual representation by alignment before projection. In *Proceedings of the 2024 conference on empirical methods in natural language processing*, pages 5971–5984, 2024. 2
- [39] Wei Liu, Fangyue Liu, Fei Ding, Qian He, and Zili Yi. Xmpfont: Self-supervised cross-modality pre-training for few-shot font generation. In *Proceedings of the IEEE/CVF conference on computer vision and pattern recognition*, pages 7905–7914, 2022. 2
- [40] Xiao-Qian Liu, Peng-Fei Zhang, Xin Luo, Zi Huang, and Xin-Shun Xu. Textadapter: Self-supervised domain adaptation for cross-domain text recognition. *IEEE Transactions on Multimedia*, 26:9854–9865, 2024. 3
- [41] Ying-Tian Liu, Zhifei Zhang, Yuan-Chen Guo, Matthew Fisher, Zhaowen Wang, and Song-Hai Zhang. Dualvector: Unsupervised vector font synthesis with dual-part representation. In *Proceedings of the IEEE/CVF Conference on Computer Vision and Pattern Recognition*, pages 14193–14202, 2023. 2
- [42] Jiasen Lu, Christopher Clark, Sangho Lee, Zichen Zhang, Savya Khosla, Ryan Marten, Derek Hoiem, and Aniruddha Kembhavi. Unified-io 2: Scaling autoregressive multimodal models with vision language audio and action. In *Proceedings of the IEEE/CVF Conference on Computer Vision and Pattern Recognition*, pages 26439–26455, 2024. 2
- [43] Yuxuan Luo, Jiaqi Tang, Chenyi Huang, Feiyang Hao, and Zhouhui Lian. Callireader: contextualizing chinese calligraphy via an embedding-aligned vision-language model. In *Proceedings of the IEEE/CVF International Conference on Computer Vision*, pages 23030–23040, 2025. 3
- [44] Xiaoxiao Ma, Mohan Zhou, Tao Liang, Yalong Bai, Tiejun Zhao, Biye Li, Huaian Chen, and Yi Jin. Star: Scale-wise text-conditioned autoregressive image generation. *arXiv preprint arXiv:2406.10797*, 2024. 2
- [45] Andrés Marafioti, Orr Zohar, Miquel Farré, Merve Noyan, Elie Bakouch, Pedro Cuenca, Cyril Zakka, Loubna Ben Allal, Anton Lozhkov, Nouamane Tazi, et al. Smolvlm: Redefining small and efficient multimodal models. *arXiv preprint arXiv:2504.05299*, 2025. 3
- [46] Wei Pan, Anna Zhu, Xinyu Zhou, Brian Kenji Iwana, and Shilin Li. Few shot font generation via transferring similarity guided global style and quantization local style. In *Proceedings of the IEEE/CVF International Conference on Computer Vision*, pages 19506–19516, 2023. 2
- [47] Song Park, Sanghyuk Chun, Junbum Cha, Bado Lee, and Hyunjung Shim. Few-shot font generation with localized style representations and factorization. In *Proceedings of the AAAI conference on artificial intelligence*, pages 2393–2402, 2021. 1, 3, 4, 5
- [48] Song Park, Sanghyuk Chun, Junbum Cha, Bado Lee, and Hyunjung Shim. Multiple heads are better than one: Few-shot font generation with multiple localized experts. In *Proceedings of the IEEE/CVF international conference on computer vision*, pages 13900–13909, 2021. 2
- [49] Niki Parmar, Ashish Vaswani, Jakob Uszkoreit, Lukasz Kaiser, Noam Shazeer, Alexander Ku, and Dustin Tran. Im-

- age transformer. In *International conference on machine learning*, pages 4055–4064. PMLR, 2018. 2
- [50] Ali Razavi, Aaron Van den Oord, and Oriol Vinyals. Generating diverse high-fidelity images with vq-vae-2. *Advances in neural information processing systems*, 32, 2019. 2
- [51] Zhihong Shao, Peiyi Wang, Qihao Zhu, Runxin Xu, Junxiao Song, Xiao Bi, Haowei Zhang, Mingchuan Zhang, YK Li, Yang Wu, et al. Deepseekmath: Pushing the limits of mathematical reasoning in open language models. *arXiv preprint arXiv:2402.03300*, 2024. 5
- [52] Wenda Shi, Yiren Song, Dengming Zhang, Jiaming Liu, and Xingxing Zou. Fonts: Text rendering with typography and style controls. In *Proceedings of the IEEE/CVF International Conference on Computer Vision*, pages 18463–18474, 2025. 3
- [53] Peize Sun, Yi Jiang, Shoufa Chen, Shilong Zhang, Bingyue Peng, Ping Luo, and Zehuan Yuan. Autoregressive model beats diffusion: Llama for scalable image generation. *arXiv preprint arXiv:2406.06525*, 2024. 2, 7
- [54] Quan Sun, Qiyong Yu, Yufeng Cui, Fan Zhang, Xiaosong Zhang, Yueze Wang, Hongcheng Gao, Jingjing Liu, Tiejun Huang, and Xinlong Wang. Emu: Generative pretraining in multimodality. *arXiv preprint arXiv:2307.05222*, 2023. 2
- [55] Licheng Tang, Yiyang Cai, Jiaming Liu, Zhibin Hong, Mingming Gong, Minhu Fan, Junyu Han, Jingtuo Liu, Errui Ding, and Jingdong Wang. Few-shot font generation by learning fine-grained local styles. In *Proceedings of the IEEE/CVF conference on computer vision and pattern recognition*, pages 7895–7904, 2022. 2, 3, 4
- [56] Shusen Tang, Zeqing Xia, Zhouhui Lian, Yingmin Tang, and Jianguo Xiao. Fontrrn: Generating large-scale chinese fonts via recurrent neural network. In *Computer Graphics Forum*, pages 567–577. Wiley Online Library, 2019. 2
- [57] Vikas Thamizharasan, Difan Liu, Shantanu Agarwal, Matthew Fisher, Michaël Gharbi, Oliver Wang, Alec Jacobson, and Evangelos Kalogerakis. Vecfusion: Vector font generation with diffusion. In *Proceedings of the IEEE/CVF conference on computer vision and pattern recognition*, pages 7943–7952, 2024. 2
- [58] Keyu Tian, Yi Jiang, Zehuan Yuan, Bingyue Peng, and Liwei Wang. Visual autoregressive modeling: Scalable image generation via next-scale prediction. *Advances in neural information processing systems*, 37:84839–84865, 2024. 2
- [59] Aaron Van Den Oord, Oriol Vinyals, et al. Neural discrete representation learning. *Advances in neural information processing systems*, 30, 2017. 2, 3
- [60] Chi Wang, Min Zhou, Tiezheng Ge, Yuning Jiang, Hujun Bao, and Weiwei Xu. Cf-font: Content fusion for few-shot font generation. In *Proceedings of the IEEE/CVF conference on computer vision and pattern recognition*, pages 1858–1867, 2023. 5
- [61] Junke Wang, Zhi Tian, Xun Wang, Xinyu Zhang, Weilin Huang, Zuxuan Wu, and Yu-Gang Jiang. Simplear: Pushing the frontier of autoregressive visual generation through pre-training, sft, and rl. *arXiv preprint arXiv:2504.11455*, 2025. 2
- [62] Xinlong Wang, Xiaosong Zhang, Zhengxiong Luo, Quan Sun, Yufeng Cui, Jinsheng Wang, Fan Zhang, Yueze Wang, Zhen Li, Qiyong Yu, et al. Emu3: Next-token prediction is all you need. *arXiv preprint arXiv:2409.18869*, 2024. 2
- [63] Yizhi Wang and Zhouhui Lian. Deepvecfont: synthesizing high-quality vector fonts via dual-modality learning. *ACM Transactions on Graphics (TOG)*, 40(6):1–15, 2021. 2
- [64] Yuqing Wang, Yizhi Wang, Longhui Yu, Yuesheng Zhu, and Zhouhui Lian. Deepvecfont-v2: Exploiting transformers to synthesize vector fonts with higher quality. In *Proceedings of the IEEE/CVF conference on computer vision and pattern recognition*, pages 18320–18328, 2023. 2
- [65] Yuqing Wang, Shuhuai Ren, Zhijie Lin, Yujin Han, Haoyuan Guo, Zhenheng Yang, Difan Zou, Jiashi Feng, and Xihui Liu. Parallelized autoregressive visual generation. In *Proceedings of the IEEE/CVF Conference on Computer Vision and Pattern Recognition*, pages 12955–12965, 2025. 2
- [66] Ze Wang, Hao Chen, Benran Hu, Jiang Liu, Ximeng Sun, Jialian Wu, Yusheng Su, Xiaodong Yu, Emad Barsoum, and Zicheng Liu. Instella-t2: Pushing the limits of 1d discrete latent space image generation. *arXiv preprint arXiv:2506.21022*, 2025. 2
- [67] Qi Wen, Shuang Li, Bingfeng Han, and Yi Yuan. Zigan: Fine-grained chinese calligraphy font generation via a few-shot style transfer approach. In *Proceedings of the 29th ACM international conference on multimedia*, pages 621–629, 2021. 2
- [68] Chenfei Wu, Jiahao Li, Jingren Zhou, Junyang Lin, Kaiyuan Gao, Kun Yan, Sheng-ming Yin, Shuai Bai, Xiao Xu, Yilei Chen, et al. Qwen-image technical report. *arXiv preprint arXiv:2508.02324*, 2025. 2
- [69] Zeqing Xia, Bojun Xiong, and Zhouhui Lian. Vecfontsd: Learning to reconstruct and synthesize high-quality vector fonts via signed distance functions. In *Proceedings of the IEEE/CVF conference on computer vision and pattern recognition*, pages 1848–1857, 2023. 2
- [70] Junfei Xiao, Zheng Xu, Alan Yuille, Shen Yan, and Boyu Wang. Palm2-vadapter: Progressively aligned language model makes a strong vision-language adapter. *arXiv preprint arXiv:2402.10896*, 2024. 3
- [71] Yangchen Xie, Xinyuan Chen, Li Sun, and Yue Lu. Dg-font: Deformable generative networks for unsupervised font generation. In *Proceedings of the IEEE/CVF conference on computer vision and pattern recognition*, pages 5130–5140, 2021. 2, 5
- [72] Zhenhua Yang, Dezhi Peng, Yuxin Kong, Yuyi Zhang, Cong Yao, and Lianwen Jin. Fontdiffuser: One-shot font generation via denoising diffusion with multi-scale content aggregation and style contrastive learning. In *Proceedings of the AAAI conference on artificial intelligence*, pages 6603–6611, 2024. 1, 2, 5
- [73] Mingshuai Yao, Yabo Zhang, Xianhui Lin, Xiaoming Li, and Wangmeng Zuo. Vq-font: Few-shot font generation with structure-aware enhancement and quantization. In *Proceedings of the AAAI Conference on Artificial Intelligence*, pages 16407–16415, 2024. 1, 2, 3, 5
- [74] Jiahui Yu, Xin Li, Jing Yu Koh, Han Zhang, Ruoming Pang, James Qin, Alexander Ku, Yuanzhong Xu, Jason Baldridge, and Yonghui Wu. Vector-quantized image modeling with improved vqgan. *arXiv preprint arXiv:2110.04627*, 2021. 2

- [75] Lili Yu, Bowen Shi, Ramakanth Pasunuru, Benjamin Muller, Olga Golovneva, Tianlu Wang, Arun Babu, Binh Tang, Brian Karrer, Shelly Sheynin, et al. Scaling autoregressive multi-modal models: Pretraining and instruction tuning. *arXiv preprint arXiv:2309.02591*, 2023. [2](#)
- [76] Qihang Yu, Mark Weber, Xueqing Deng, Xiaohui Shen, Daniel Cremers, and Liang-Chieh Chen. An image is worth 32 tokens for reconstruction and generation. *Advances in Neural Information Processing Systems*, 37:128940–128966, 2024. [1](#), [2](#)
- [77] Qihang Yu, Ju He, Xueqing Deng, Xiaohui Shen, and Liang-Chieh Chen. Randomized autoregressive visual generation. In *Proceedings of the IEEE/CVF International Conference on Computer Vision*, pages 18431–18441, 2025. [2](#)
- [78] Kaiwen Zha, Lijun Yu, Alireza Fathi, David A Ross, Cordelia Schmid, Dina Katabi, and Xiuye Gu. Language-guided image tokenization for generation. In *Proceedings of the Computer Vision and Pattern Recognition Conference*, pages 15713–15722, 2025. [2](#)
- [79] Yexun Zhang, Ya Zhang, and Wenbin Cai. Separating style and content for generalized style transfer. In *Proceedings of the IEEE conference on computer vision and pattern recognition*, pages 8447–8455, 2018. [2](#)
- [80] Yexun Zhang, Ya Zhang, and Wenbin Cai. Separating style and content for generalized style transfer. In *Proceedings of the IEEE conference on computer vision and pattern recognition*, pages 8447–8455, 2018. [2](#)
- [81] Anlin Zheng, Haochen Wang, Yucheng Zhao, Weipeng Deng, Tiancai Wang, Xiangyu Zhang, and Xiaojuan Qi. Holistic tokenizer for autoregressive image generation. In *Proceedings of the IEEE/CVF International Conference on Computer Vision*, pages 16916–16926, 2025. [2](#)